JACS
JOURNAL OF THE AMERICAN CHEMICAL SOCIETY
pubs.acs.org/JACS
Article

Beyond the Vibrational Stark Effect: Unraveling the Large Redshifts of Alkyne C−H Bond in Solvation Environments

Chu Zheng,[#] Yuezhi Mao,[#] Thomas E. Markland,[*] and Steven G. Boxer[*]

Cite This: J. Am. Chem. Soc. 2025, 147, 6227−6235
Read Online

ABSTRACT: C−H···O hydrogen bonds are formed in systems ranging from biomolecular complexes to small-molecule structures. Previous work has focused on the blueshifts in the C−H stretching frequency ($\bar{\nu}_{CH}$) induced by these hydrogen bonds and their chemical and biological roles. Here, we show that, in contrast, terminal alkyne C−H hydrogen bonds exhibit large redshifts (50−100 cm^{-1}) upon hydrogen bonding with oxygen-containing solvents. Using spectroscopic and computational approaches, we elucidate and compare the roles of the vibrational Stark effect, bond polarization, and charge transfer in driving the C−H redshift. We show that the redshifts of alkyne's terminal C−H upon the formation of hydrogen bonds correlate with the Lewis basicity of the solvent and are significantly larger than those arising solely from solvent electric fields (vibrational Stark effect), differing from the well-studied redshift of carbonyl vibrations induced by hydrogen bonds. Through a decomposition of vibrational frequency shifts based on DFT calculations using absolutely localized molecular orbitals, we demonstrate that including the effects of bond polarization and charge transfer, in addition to the vibrational Stark effect, results in quantitative agreement between experimentally observed C−H frequency shifts and the theoretically predicted values in various oxygen-containing solvents. Our results highlight the significance of effects beyond pure electrostatics in accounting for the large redshifts in C−H···O hydrogen bonds and exemplify our approach to quantifying the contributions from different physical effects.

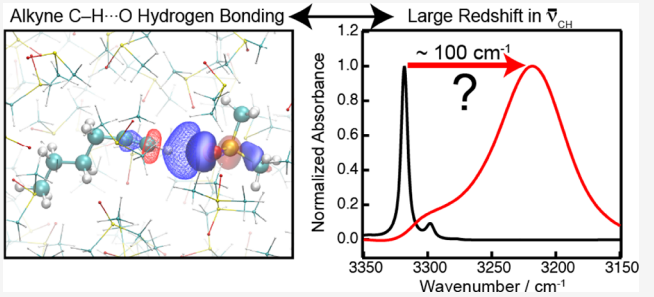

INTRODUCTION

Nonclassical hydrogen bonds (HB) involving carbon−hydrogen (C−H) bonds[1,2] are widely present at hydrophobic interfaces and in biomolecular interactions.[3−5] The weak bond polarity of C−H bonds compared to typical hydrogen bond donors and the varying bonding environments of carbon atoms enable them to provide a diverse range of interactions, which, in addition to their biological relevance[3,6,7] show promise in designing synthetic structures with novel functions and properties.[8−10] Previous research has focused on C−H···O hydrogen bonds,[11−16] which typically exhibit a blueshift of a few to a few tens of cm^{-1} in the C−H stretching frequency. Theoretical analyses based on electronic structure calculations attribute the observed blueshift to the sterically induced contraction of the C−H bond in C−H···O hydrogen bonds.[11−13,17−19] However, several other possible origins for the blueshifts have also been proposed.[12,20−30] In contrast, redshifts in the C−H bond frequency arising from C−H···O interactions have not been systematically investigated.[1] In this work, we show that terminal alkyne C−H bonds undergo substantial redshifts (50−100 cm^{-1}) upon the formation of hydrogen bonds with oxygen-containing solvents such as DMSO (Figure 1A,B) and elucidate the underlying mechanisms via a combined spectroscopic and computational study. In particular, we consider whether the redshifts observed for the terminal alkyne C−H frequencies arise from a similar electrostatic basis as in the case of carbonyl (C═O) vibrations, where the bond-stretching frequency exhibits a linear correlation with the electric field exerted by the environment along the bond[31] and thus is dominated by the vibrational Stark effect (VSE). We show that when C−H···O hydrogen bonds are formed, bond polarization and charge transfer (Figure 1C) contribute significantly to the redshift in C−H, in addition to the VSE. This reveals a striking difference between the physical origins of C−H redshifts as a proton donor and the previously reported redshifts in C═O as a proton acceptor in hydrogen-bonding environments.

RESULTS

To elucidate the physical origins of the C−H bond frequency shift in solution, we first quantified the electrostatic effect on

Received: December 22, 2024
Revised: January 29, 2025
Accepted: February 3, 2025
Published: February 10, 2025

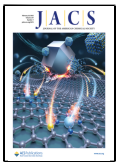

https://doi.org/10.1021/jacs.4c18102
J. Am. Chem. Soc. 2025, 147, 6227−6235

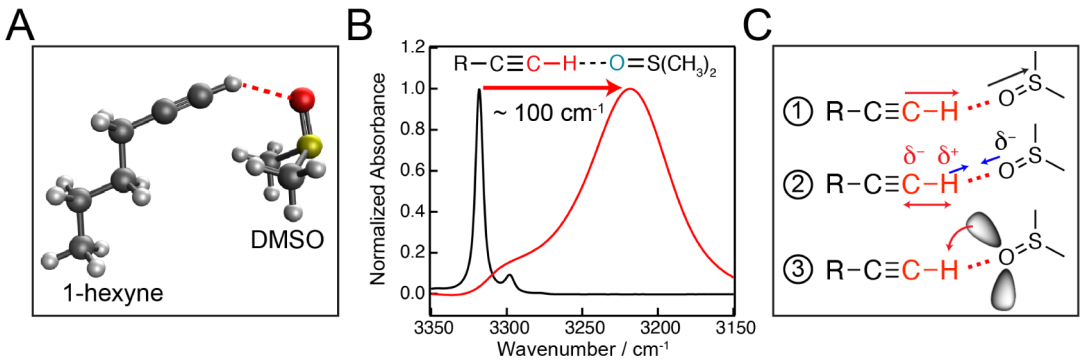

Figure 1. C−H···O hydrogen bond between alkyne terminal C−H and DMSO. (A) Computationally optimized structure of the 1-hexyne:DMSO dimer complex featuring the C−H···O hydrogen bond. (B) Experimental IR spectra showing the substantial redshift of 100 cm^{-1} in 1-hexyne's terminal C−H stretching frequency in DMSO (red) relative to that in hexane (black) due to the C−H···O hydrogen bond with DMSO. (C) Schematic of physical effects that may contribute to the redshift of C−H observed in DMSO, including the vibrational Stark effect (①), C−H bond polarization (②), and charge transfer from the lone electron pair of oxygen to σ^* of the C−H bond (③). In ①, the red and black arrows represent the bond dipoles of the terminal C−H bond and the S═O bond, respectively. The DMSO molecules surrounding the alkyne solute exert an electric field on the C−H bond, which can result in a redshift known as the vibrational Stark effect. In ②, the red and blue arrows illustrate the elongation of the C−H bond and the reduction in distance between the H and O atoms due to bond polarization, respectively, which can lower the C−H stretching vibrational force constant and lead to a redshift. In ③, the red arrow shows interactions between the lone pair of the O atom and the σ^* antibonding orbital associated with the C−H bond.

the C−H vibrational frequency ($\bar{\nu}_{CH}$) experimentally by using vibrational Stark spectroscopy (VSS). We then combined vibrational solvatochromism measurements and molecular dynamics (MD) simulations to demonstrate the substantial deviation of the experimentally observed shifts in $\bar{\nu}_{CH}$ from those predicted by the linear vibrational Stark effect for solvents that can form C−H···O hydrogen bonds. By performing DFT-based adiabatic energy decomposition analysis (aEDA) for the model hydrogen-bond complexes, we further show that the inclusion of bond polarization and charge transfer results in close agreement with the experimentally observed frequency shifts, suggesting their key role in driving the large $\bar{\nu}_{CH}$ shift in C−H···O hydrogen bonds.

Vibrational Stark Spectroscopy. We used vibrational Stark spectroscopy[32,33] to directly measure the $\bar{\nu}_{CH}$ shift in response to an externally applied electric field and to establish the origins of this response as arising from the dipole difference between the vibrational ground and excited states. Figure 2 shows the IR absorption and the corresponding vibrational Stark spectra of 1-hexyne in 2-methyl THF at 77 K. As shown in Figure 2A, the C−H stretch of 1-hexyne shows a single band. The vibrational Stark spectrum (Figure 2B), which is a difference spectrum between the field-on and field-off absorbances, shows the dominance of the second-derivative of the absorption line shape. Similar spectral results were observed for phenylacetylene (Figure S1).

The dominant second-derivative line shape of the vibrational Stark spectra indicates that the response of $\bar{\nu}_{CH}$ to an electric field primarily arises from the C−H vibration's difference dipole, $|\Delta\vec{\mu}_{CH}|$. This leads to a linear frequency response to electric fields: $\Delta\bar{\nu}_{CH} = -|\Delta\vec{\mu}_{CH}|F_{CH}$, where $\Delta\bar{\nu}_{CH}$ and F_{CH} refer to the C−H frequency shift and the electric field exerted on the C−H bond (which is defined as the average of field projections on the two bonding atoms), respectively. $|\Delta\vec{\mu}_{CH}|$, also known as the Stark tuning rate, is an indicator of the intrinsic sensitivity of a vibrational probe to electric fields. From the second derivative contribution, we obtained Stark tuning rates of C−H, which are 3.13/f and 3.83/f cm^{-1}/(MV/cm) for 1-hexyne and phenylacetylene, respectively (Table S1). The unitless

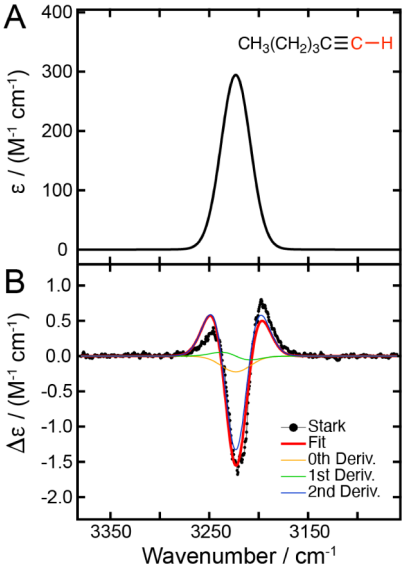

Figure 2. Vibrational Stark spectroscopy of 1-hexyne. (A) The IR absorption spectrum of the terminal C−H vibration of 1-hexyne (200 mM) in 2-methyl THF at 77 K. (B) The vibrational Stark spectrum of the terminal C−H vibration ($\Delta\varepsilon$ stands for the difference between the field-on and field-off molar absorptivities), scaled to an applied electric field of 1.0 MV/cm with best fits and the 0th, first, and second derivative contributions (Table S1).

local field factor f reflects the difference between the applied field and the actual field experienced by C−H. Although the exact value of f is influenced by the polarization of the frozen glass matrix that creates the local field effect, previous studies have shown that f is approximately 2 for various glass-forming solvents,[31,34,35] including 2-methyl THF used in this study. These Stark tuning rates of the alkyne C−H are larger than those of the well-studied C═O and C≡N probes,[31] whose $|\Delta\vec{\mu}_{CH}|$'s are ~1−2/f cm^{-1}/(MV/cm), but are similar to the values for O−H,[36] S−H, and N−H,[37] indicating the high sensitivity of alkyne's terminal C−H to electric fields.

https://doi.org/10.1021/jacs.4c18102
J. Am. Chem. Soc. 2025, 147, 6227−6235

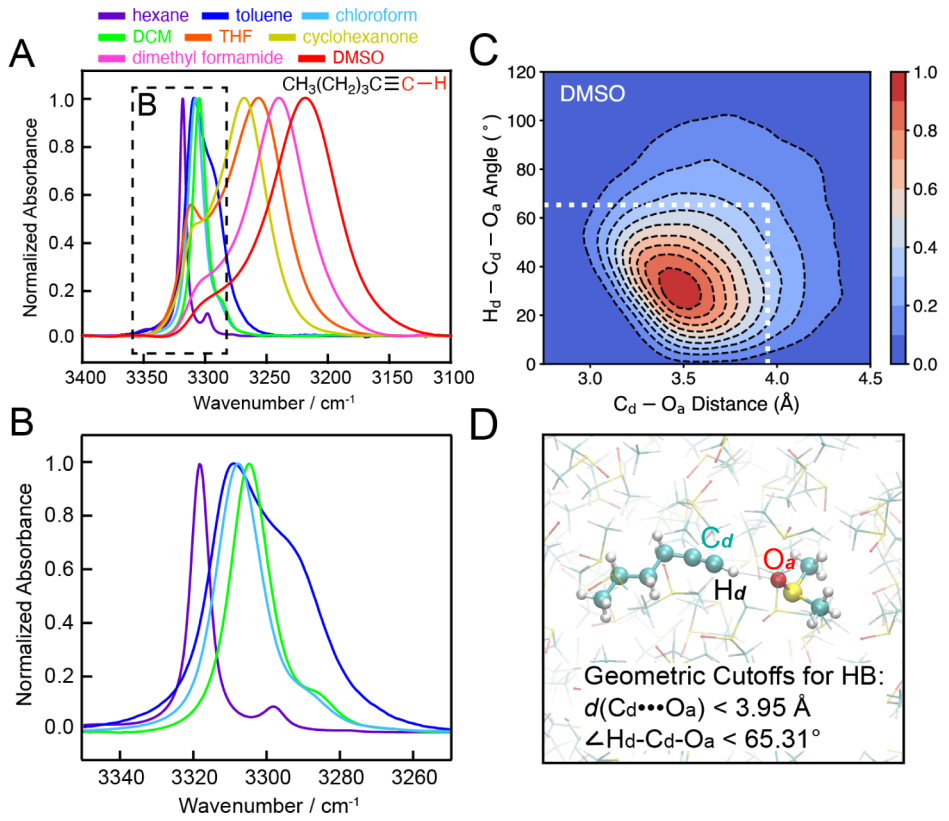

Figure 3. Vibrational solvatochromism of 1-hexyne. (A) Normalized experimental IR spectra of 20 mM 1-hexyne in oxygen-containing solvents, showing significant redshifts in the terminal C−H stretch. A shoulder peak around 3300 cm^{-1} is observed across all solvents, which has previously been assigned as a Fermi resonance between the terminal C−H stretch fundamental and the combination of the first overtone of the terminal C−H bend and the C≡C stretch fundamental.[60,61] In the case of toluene, the more pronounced shoulder peak may also arise from C−H···π interactions between the alkyne C−H and toluene as supported by DFT frequency calculations (Figure S10). The frequencies of these shoulder peaks in oxygen-containing solvents do not correlate with the average solvent electric fields experienced by the non-HB population of alkyne in these solvents (Figure S11). (B) Normalized experimental IR spectra of 20 mM 1-hexyne in nonoxygen-containing solvents with varying polarities. (C) Normalized two-dimensional probability density distribution $P[d(C_d{-}O_a), \angle H_d{-}C_d{-}O_a]/P_{max}$ for configurations sampled from MD simulations, where $d(C_d{-}O_a)$ (the x-axis) represents the distance between the C atom of terminal alkyne and the O atom of DMSO, and $\angle H_d{-}C_d{-}O_a$ (the y-axis) represents the angle between the C−H bond vector and the $C_d{\cdots}O_a$ axis. The white dotted lines indicate the distance and angle cutoffs for C−H···O HBs employed in this work, and the bottom left region of the graph corresponds to the HB configurations. (D) A snapshot from the MD simulations illustrating the C−H···O hydrogen bond formed between 1-hexyne (solute) and DMSO (solvent).

Vibrational Solvatochromism of Alkyne C−H. Having established the redshift of the terminal alkyne C−H frequency in response to an applied field, we now consider its response to electric fields produced by solvent environments (vibrational solvatochromism). Across a range of solvents, the terminal C−H vibrational frequency of 1-hexyne shows a redshift as the solvent polarity increases (Figure 3A,B, Table S2 and S3), following a trend similar to that observed for C=O vibrational probes.[31,34] While $\bar{\nu}_{CH}$ undergoes a moderate 13 cm^{-1} redshift from hexane to DCM, we observed more prominent redshifts of 50−100 cm^{-1} (relative to $\bar{\nu}_{CH}$ in hexane) in the four oxygen-containing solvents. These redshifts are significantly larger in magnitude than those observed in the C=O or C≡N probes studied to date, which typically exhibit a redshift of 10−30 cm^{-1} from hexane to DMSO,[31,35] and are also in stark contrast with the solvatochromic blueshift (~10 cm^{-1} from hexane to DMSO) of an aldehyde C−D reported in our prior work.[38] We attribute these large redshifts in the C−H stretching frequency to the formation of C−H···O hydrogen bonds in the oxygen-containing solvents, contrasting with C=O and C≡N probes that do not form hydrogen bonds with aprotic solvents like those used in this study.

To provide insights into the geometry of the C−H···O hydrogen bonds formed between 1-hexyne and the solvents, we performed MD simulations for these systems (see Method S3 for details). As shown in Figure 3C, from the MD trajectories, we obtained a probability density distribution of the $H_d{-}C_d{-}O_a$ angle ($\angle H_d{-}C_d{-}O_a$) and the $C_d{-}O_a$ distance, $d(C_d{-}O_a)$. Here, $\angle H_d{-}C_d{-}O_a$ refers to the angle between the C−H bond vector and the C···O axis, and $d(C_d{-}O_a)$ refers to the distance between the terminal C atom of the alkyne and the O atom of the solvent (Figure 3D). The most probable values of $\angle H_d{-}C_d{-}O_a$ and $d(C_d{-}O_a)$ for 1-hexyne in DMSO are 33.7° and 3.5 Å (Figures S2, S3 and Table S4), respectively. Figure 3D shows a simulation snapshot from the most probable region in Figure 3C, illustrating a representative geometrical configuration that features a C−H···O hydrogen bond. In comparison to hydrogen bonds in liquid water, which are typically identified based on the criteria $d(O_d{-}O_a)$ < 3.5 Å and $\angle H_d{-}O_d{-}O_a$ < 30°,[39] the C−H···O hydrogen bond between 1-hexyne and DMSO features larger donor−acceptor distances and diminished linearity due to the weaker interaction.

Deviation from the Linear Vibrational Stark Effect in Oxygen-Containing Solvents. To quantify how electro-

https://doi.org/10.1021/jacs.4c18102
J. Am. Chem. Soc. 2025, 147, 6227−6235

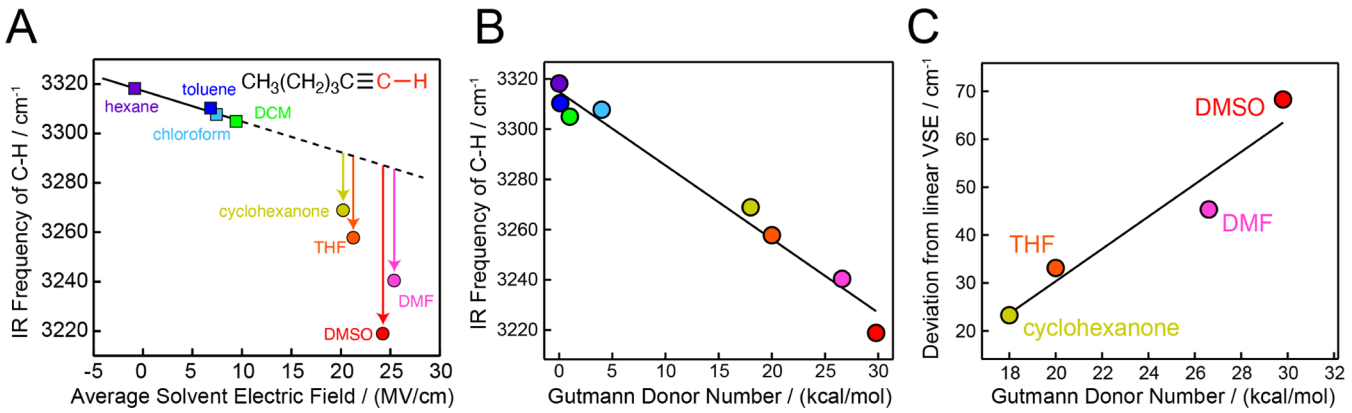

Figure 4. IR frequency of the alkyne's terminal C−H in oxygen-containing solvents deviates from the linear VSE but shows a strong correlation with solvent basicity. (A) Correlation between the measured IR frequency of 1-hexyne's terminal C−H stretch and the average solvent electric fields on the C−H bond, obtained from QM calculations performed on the MD-sampled configurations (see Method S4 for details). The frequencies correspond to the peak maxima positions in Figure 3A. The squares represent nonoxygen-containing solvents. The circles represent oxygen-containing solvents (Table S5). The least-squares linear fitting, based on the frequency ($\bar{\nu}_{CH}$) and field (F_{CH}) results for the nonoxygen-containing solvents, yields $\bar{\nu}_{CH} = -1.25F_{CH} + 3317.4$ ($R^2 = 0.97$). Arrows represent the deviation of the measured C−H stretching frequency from the extrapolated values of the linear VSE in each oxygen-containing solvent. (B) Linear correlation between the IR frequency of C−H ($\bar{\nu}_{CH}$) and the Gutmann donor number (D_N) of all eight solvents investigated in this study. The least-squares linear fitting gives $\bar{\nu}_{CH} = -2.94D_N + 3314.4$ ($R^2 = 0.98$). (C) Linear correlation between the deviation of $\Delta\bar{\nu}_{CH}$ from the linear VSE (represented by the arrows in panel A) and D_N of each oxygen-containing solvent. The least-squares linear fitting gives $\Delta\bar{\nu}_{CH} = 3.4D_N - 37.2$ ($R^2 = 0.93$).

static interactions contribute to the solvatochromic shifts in $\bar{\nu}_{CH}$, we calculated the average solvent electric fields exerted on the C−H bond (Table S5 and Method S4). Focusing on the four non-HB solvents first, as shown in Figure 4A, $\bar{\nu}_{CH}$ shows a linear correlation with the average solvent electric field, suggesting that the redshifts in $\bar{\nu}_{CH}$ can be accounted for under the framework of the linear VSE. The gradient of the line in Figure 4A, 1.25 $cm^{-1}/(MV/cm)$, gives the Stark tuning rate $|\Delta\vec{\mu}_{CH}|$. This value was measured to be $3.13/f$ $cm^{-1}/(MV/cm)$ by VSS (Figure 2B), and thus the local field factor f here is around 2.5, similar to values reported in the literature for C═O and C≡N vibrational probes.[31,34,35] Note that the positive electric field on C−H stabilizes the bond dipole, leading to a redshift in $\bar{\nu}_{CH}$, which is opposite to the case of C═O. This is because a field in the C→H direction is aligned with the C−H bond dipole, whereas a field in the C→O direction is antiparallel with the C═O bond dipole (Figure S4). In agreement with the VSS results, the Stark tuning rate of 1.25 $cm^{-1}/(MV/cm)$ obtained from the field-frequency correlation is also much larger than the values of the C═O and C≡N probes previously studied,[31] which usually fall between 0.2 and 0.6 $cm^{-1}/(MV/cm)$. This large $|\Delta\vec{\mu}_{CH}|$ further corroborates the high sensitivity of the alkyne C−H vibrational frequency to electric fields, compared to other vibrational probes.

To calculate the average solvent electric fields experienced by the hydrogen-bonded alkyne C−H in oxygen-containing solvents, we extracted MD snapshots satisfying the geometric criterion for HBs ($d(C_d{-}O_a) < 3.95$ Å and $\angle H_d{-}C_d{-}O_a < 65.31°$) as illustrated in Figure 3C. These cutoff values were determined as the maximum values of $d(C_d{-}O_a)$ and $\angle H_d{-}C_d{-}O_a$ on the contour line corresponding to $P[d(C_d{-}O_a), \angle H_d{-}C_d{-}O_a]/P_{max} = 1/e \approx 0.368$, where P stands for probability density calculated from the MD trajectory for 1-hexyne in DMSO (see Section S6 for additional details).[40] At the simulation temperature (300 K), this criterion yields hydrogen bonds within ~0.6 kcal/mol of the lowest free energy HB configuration. We observed a correlation between the linewidth of the C−H vibration and the calculated standard deviation of solvent electric fields (Figure S5) in both the non-HB and HB solvents, similar to previous studies of C═O,[35] confirming that the linewidth observed primarily arises from inhomogeneous broadening. As shown in Figure 4A, although the solvent electric fields calculated using the HB configurations for the oxygen-containing solvents are larger than the fields calculated as full-ensemble averages (Figure S6) and those in nonoxygen-containing solvents, as expected, the large redshifts in $\bar{\nu}_{CH}$ significantly deviate from the fitted line representing the linear VSE. This deviation is unlikely to result from a significant change in $|\Delta\vec{\mu}_{CH}|$ upon the formation of C−H···O hydrogen bonds, given that the measured $|\Delta\vec{\mu}_{CH}|$ of the hydrogen-bonded C−H in the frozen glass of 2-methyl THF by VSS is similar to that in non-HB solvents, assuming $f \approx 2.5$ (Figures 2 and 4A). Since THF and 2-methyl THF have analogous chemical structures and exhibit similar dielectric constants (ε = 7.4 and 7.0 for THF and 2-methyl THF, respectively) as well as vibrational solvatochromism for alkyne C−H (Figure S7), we expect a similar Stark tuning rate $|\Delta\vec{\mu}_{CH}|$ to apply in THF and other oxygen-containing solvents. Together, these results indicate that additional factors other than electrostatics play a crucial role in red-shifting $\bar{\nu}_{CH}$ upon the formation of C−H···O hydrogen bonds, in intriguing contrast with C═O probes, for which linear field-frequency correlations hold in both non-HB and HB environments.[35]

In contrast to the nonlinearity shown in Figure 4A, we obtained a linear correlation between $\bar{\nu}_{CH}$ and the Gutmann donor number of each solvent, across both non-HB and HB solvent environments (Figure 4B). The Gutmann donor number[41] is a widely used empirical parameter for quantifying the strength of solvents as Lewis bases, defined by the formation enthalpy of a 1:1 adduct between antimony pentachloride ($SbCl_5$) and the solvent of interest. Hence, the linear correlation shown in Figure 4B indicates the key role of the solvent's Lewis basicity in driving C−H frequency shifts.

https://doi.org/10.1021/jacs.4c18102
J. Am. Chem. Soc. 2025, 147, 6227−6235

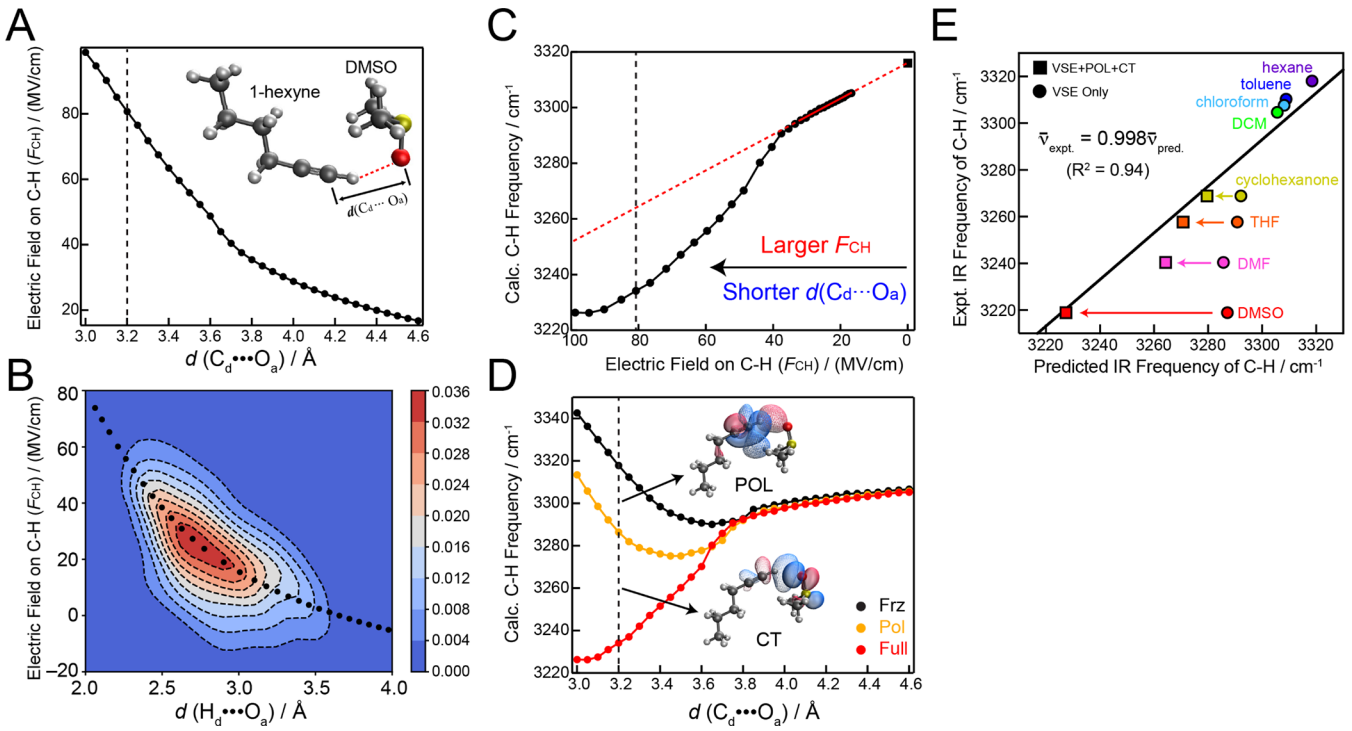

Figure 5. Computational analysis of the contributions from bond polarization and charge transfer to the large redshift of $\bar{\nu}_{CH}$ upon the formation of C−H···O hydrogen bonds. (A) The projection of the DMSO-induced electric field on the terminal C−H (F_{CH}) calculated (Method S4) in the course of the scan of the C_d···O_a distance (labeled in inset). The vertical dashed line at 3.2 Å represents the C_d···O_a distance within the optimized HB complex structure. (B) Comparison of electric fields on C−H calculated (i) along the H_d···O_a distance scan within the 1-hexyne:DMSO model complex (black dots) and (ii) using MD-sampled configurations for four oxygen-containing solvents (shown as contour lines, which are generated based on the statistics of F_{CH} and $d(H_d···O_a)$, evaluated on 400 MD snapshots). The electric field values for the model HB complex at different distances are universally shifted by −25 MV/cm to match the most probable field strength in solvent at varying H_d···O_a distances. (C) Correlation between the calculated $\bar{\nu}_{CH}$ and electric field on C−H at varying distances. The least-squares fit for the region of $d(C_d···O_a)$ > 3.7 Å gives $\bar{\nu}_{CH} = -0.65F_{CH} + 3316.2$ ($R^2 = 0.997$). The black square at F_{CH} = 0 MV/cm shows the computed $\bar{\nu}_{CH}$ of an isolated 1-hexyne molecule, which serves as a cross validation at the zero-field limit and was not included in fitting. The vertical dashed line represents the electric field value at the same equilibrium distance as in panel A. (D) Adiabatic energy decomposition analysis (aEDA) for the shift in $\bar{\nu}_{CH}$, which was performed at varying intermolecular C_d···O_a distances for the 1-hexyne:DMSO complex (Method S5). The vertical dashed line represents the same equilibrium distance as in panel A. The inset shows the orbitals dominating the polarization (POL) and charge-transfer (CT) processes, with the solid and meshed orbitals corresponding to the occupied and virtual orbitals, respectively. (E) Linear correlation between the experimentally measured IR frequencies ($\bar{\nu}_{CH}$) and the predicted values, including contributions from the VSE, bond polarization, and charge transfer. A least-squares fit with a line passing through the origin gives $\bar{\nu}_{expt.} = 0.998\bar{\nu}_{pred.}$ ($R^2 = 0.94$). For the oxygen-containing solvents, the horizontal arrows correspond to the combined POL and CT contributions to the redshifts as quantified using aEDA (Table S7).

Moreover, for the oxygen-containing solvents, the deviations of the $\bar{\nu}_{CH}$ values from the fitted VSE line (indicated by the arrows in Figure 4A) also exhibit a strong linear correlation with their Gutmann donor numbers (Figure 4C), suggesting that the additional factors beyond VSE that contribute to the large C−H redshifts are correlated with the Lewis basicity of solvents. Based on these observations and the smaller intrinsic dipole of C−H compared to C═O, we hypothesize that C−H bond polarization through C−H···O interactions, as well as charge transfer[42−44] from the lone pair of the solvent oxygen atom to the antibonding σ^* orbital of C−H,[42−45] can weaken the C−H bond and thus significantly red-shift $\bar{\nu}_{CH}$.[13]

Bond Polarization and Charge Transfer Across C−H··· O Hydrogen Bonds. To understand the substantial deviations from linear VSE in oxygen-containing solvents (Figure 4A), we employed quantum mechanical (QM) calculations to investigate a model complex (the hydrogen-bonded 1-hexyne:DMSO complex; shown in the inset of Figure 5A) to quantify the contributions of bond polarization and charge transfer to the large redshifts in $\bar{\nu}_{CH}$. Starting from the optimized complex structure where 1-hexyne's terminal C−H forms a stable hydrogen bond with DMSO at $d(C_d···O_a)$ = 3.2 Å, we performed a scan of the intermolecular distance along the C_d···O_a axis and investigated how the C−H stretching frequency ($\bar{\nu}_{CH}$) and the electric field exerted on C−H (F_{CH}) are predicted to vary upon the formation of the C−H···O hydrogen bond. At each distance, we calculated F_{CH} using two distinct electronic structure partitioning methods,[38] subsystem-projected atomic orbital decomposition (SPADE)[46] and absolutely localized molecular orbitals (ALMO),[47] which yielded similar results (Figure S8 and Table S6). We thus focus on the SPADE results in the discussion below.

As shown in Figure 5A, F_{CH} increases monotonically as $d(C_d···O_a)$ decreases, with the slope becoming notably steeper when $d(C_d···O_a)$ is at 3.7 Å or below. We further investigated the variation of F_{CH} with $d(H_d···O_a)$, the distance between the donor H and acceptor O, along the intermolecular distance scan. The resulting trend is compared to the distribution of F_{CH} with respect to $d(H_d···O_a)$ calculated based on MD-sampled configurations for all four oxygen-containing solvents

https://doi.org/10.1021/jacs.4c18102
J. Am. Chem. Soc. 2025, 147, 6227−6235

using the SPADE partitioning method. We note that the same set of MD snapshots was used to compute the ensemble-averaged field values in Figure 4A. Figure 5B shows that with a constant shift of −25 MV/cm applied to the electric field values calculated along the intermolecular distance scan, the resulting values (as indicated by the black dots) closely capture the overall trend of F_{CH} vs $d(H_d\cdots O_a)$ obtained from the MD simulations. This supports the relevance of this simple model complex to the HBs in the more complicated solvent environments. The discrepancy in the electric field strengths, manifested by the need for the −25 MV/cm shift, likely reflects the solvent screening effect on electrostatic interactions, which reduces the fields obtained from the MD simulations.

Figure 5C shows a linear correlation between $\overline{\nu}_{CH}$ and F_{CH} calculated for the model complex when the field is below 40 MV/cm, corresponding to $d(C_d\cdots O_a) > 3.7$ Å. This linear correlation allows for the extrapolation of $\overline{\nu}_{CH}$ to $F_{CH} = 0$, yielding $\overline{\nu}_{CH}(F = 0) = 3316.2$ cm^{-1}, which is in excellent agreement with 3316.0 cm^{-1}, the calculated gas-phase $\overline{\nu}_{CH}$ for 1-hexyne. Notably, these results also align well with the zero-field $\overline{\nu}_{CH}$ (3317.4 cm^{-1}) extrapolated from the linear field-frequency correlation observed in solvatochromism, as shown in Figure 4A. These findings show the dominance of the linear VSE in the long range where the HB donor and acceptor are well-separated. However, as the intermolecular distance decreases, $\overline{\nu}_{CH}$ starts to deviate from this linear correlation: at the equilibrium complex structure where $d(C_d\cdots O_a) = 3.2$ Å, $\overline{\nu}_{CH}$ deviates from the trend of linear VSE toward the red end (lower frequency) by approximately 30 cm^{-1}, which qualitatively aligns with the experimentally observed redshift (Figure 4A).

To identify the physical origin of this deviation from the VSE, we used the adiabatic energy decomposition analysis (aEDA) method[48,49] with $d(C_d\cdots O_a)$ constrained at the same set of values (Method S5). This approach calculates $\overline{\nu}_{CH}$ at the optimized geometries on three potential energy surfaces: the frozen (Frz), polarized (Pol), and full (Full) surfaces. On the Frz surface, the electronic structure of each monomer remains unchanged as they would in isolation. Consequently, the bond polarization and charge transfer effects are decoupled. The shift in $\overline{\nu}_{CH}$ from the Frz surface to the Pol surface corresponds to the contribution of bond polarization, and the further shift from the Pol surface to the Full surface reflects the contribution of charge transfer. As shown in Figure 5D, the curves for the frozen, polarized, and fully relaxed surfaces largely overlap when $d(C_d\cdots O_a) > 3.7$ Å, indicating minimal contributions from bond polarization and charge transfer. Correspondingly, the vibrational frequency shifts in this region can be well captured by the VSE as shown in Figure 5C. As $d(C_d\cdots O_a)$ decreases, bond polarization and charge transfer both contribute significantly to the redshift in $\overline{\nu}_{CH}$, accounting for the substantial deviation from the linear VSE. These effects both cause red-shifting because they enhance the σ^* character of C−H, which is revealed by the dominant complementary occupied-virtual pairs (COVPs)[50,51] associated with the polarization and charge-transfer processes (insets of Figure 5D). We also note that without the effects of bond polarization and charge transfer, $\overline{\nu}_{CH}$ would be blue-shifted in the short range due to the effect of Pauli repulsion, which was identified as the origin of blue-shifting HBs involving C(sp^3)−H.[11−13,17−19] In contrast, the much stronger bond polarization and charge-transfer effects experienced by the more acidic alkyne C−H outweigh the effect of Pauli repulsion, resulting in large redshifts instead.

Given that $\overline{\nu}_{CH}$ shows a deviation from the linear VSE in solvents in the increasing order: cyclohexanone, THF, DMF, and DMSO (Figure 4A,C), we investigated whether this trend arises from the varying magnitude of contributions from bond polarization and charge transfer for each solvent. Using aEDA, we calculated these contributions to the redshift in $\overline{\nu}_{CH}$ (Table S7) when 1-hexyne is hydrogen-bonded to the four oxygen-containing solvents under the minimum-energy complex structures (Figure S9). This yielded additional shifts beyond VSE, $\Delta\overline{\nu}_{CH,POL+CT}$ of −12.5, −20.1, −21.4, and −59.7 cm^{-1} for cyclohexanone, THF, DMF, and DMSO, respectively. Figure 5E shows the frequencies ("VSE only", circles) that would be expected if the linear VSE trend in Figure 4A (dashed line) was followed. For each of the oxygen-containing solvents, this accounts for a shift of around −30 cm^{-1} from the zero-field frequency (3317.4 cm^{-1}), whereas the experimentally observed frequencies are red-shifted even further in comparison. Adding the computationally obtained shifts for the effects of polarization and charge transfer ($\Delta\overline{\nu}_{CH,POL+CT}$) that go beyond the simple VSE picture (yielding "VSE+POL +CT", squares), one achieves excellent agreement with the experimentally observed frequencies ($R^2 = 0.94$, with a slope of 0.998). This agreement strongly suggests that the large redshifts in $\overline{\nu}_{CH}$ observed in oxygen-containing solvents should be attributed to a combination of all three effects illustrated in Figure 1C: VSE, bond polarization, and charge transfer. Further, this demonstrates that an accurate correction for the effects beyond VSE could be obtained using aEDA for different hydrogen-bonding solvents from just the minimum-energy complex structure, providing a very convenient and efficient route for including or removing the non-VSE contributions in other systems.

DISCUSSION

The significant redshift observed for the terminal alkyne C−H in DMSO contrasts with the blueshift previously observed for an aldehyde C−D probe,[38] which arises from fundamentally different physical origins. In the case of aldehyde C−D, the deuteron is more electronegative than the carbonyl carbon due to the electron-withdrawing effect of the carbonyl oxygen. As a result, aldehyde C−D cannot form hydrogen bonds with oxygen-containing solvents. Instead, its frequency shift is primarily driven by the VSE, and it experiences a destabilizing (blue-shifting) solvent electric field that preferentially stabilizes the more pronounced carbonyl bond dipole. In contrast, the Lewis acidic nature of the terminal alkyne's C−H allows it to form C−H···O hydrogen bonds with oxygen-containing solvents, leading to significant redshifts, as demonstrated in this work.

The striking difference between C−H and C═O probes highlights the more substantial impact of bond polarization and charge transfer on the vibrational properties of the former compared to the latter. This can be rationalized by invoking the concept of bond order: for C═O, which serves as a proton acceptor, the bond polarization and charge transfer primarily involve the nonbonding orbitals (lone pairs of oxygen), thus having a limited impact on the bond strength; in contrast, for C−H that serves as a proton donor, bond polarization and charge transfer enhance the partial occupation of the σ^* orbital, resulting in more pronounced changes in the bond-

https://doi.org/10.1021/jacs.4c18102
J. Am. Chem. Soc. 2025, 147, 6227−6235

stretching frequency. Additionally, the behavior of the alkyne C−H probe also differs markedly from that of the C≡N group, another widely used vibrational probe that can serve as a proton acceptor. While the formation of HBs typically blue-shifts the vibrational frequency of C≡N, canceling out the redshift caused by VSE,[52−56] bond polarization and charge transfer upon the formation of alkyne C−H···O HBs, in combination with the VSE, produces substantial redshifts.

CONCLUSIONS

In summary, we have shown that the terminal alkyne C−H bond is sensitive to electric fields, and its frequency shift in non-HB environments can be explained under the vibrational Stark effect. However, the formation of C−H···O hydrogen bonds with oxygen-containing solvents can induce a large redshift in the C−H vibration, and in contrast to carbonyl-based vibrational probes, this large redshift cannot be solely attributed to the linear VSE but rather involves substantial contributions from bond polarization and charge transfer facilitated by the hydrogen bond. Using a combined experimental and computational approach, we quantified the individual contributions of these physical effects to the overall frequency shifts and elucidated the distinct characteristics of alkyne C−H compared to other widely used (C═O and C≡N) or recently reported (aldehyde C−D) vibrational probes.

The ability to incorporate alkyne probes into chemical and biomolecular systems through amber suppression or site-specific functionalization strategies utilized in click chemistry opens exciting possibilities for their application as vibrational probes in energy and biological sciences.[57−59] The unique features of alkyne C−H demonstrated herein provide complementary insights into the electrostatics and Lewis basicity of local chemical environments, expanding on the prior focus on the C≡C vibration. Furthermore, the integrative approach we present in this work provides a framework for understanding the physical basis of C−H-involved hydrogen bonds or any noncovalent interaction probed by vibrational frequency shifts.

ASSOCIATED CONTENT

Supporting Information

The Supporting Information is available free of charge at https://pubs.acs.org/doi/10.1021/jacs.4c18102.

Materials and methods, Figures S1−S11, and Tables S1−S8; computational data, including force field parameters and stationary structures obtained from or used for electronic structure calculations (PDF)

XYZ coordinates of truncated MD snapshots for solvent electric field calculations and those generated from the intermolecular distance scan of the 1-hexyne:DMSO complex (ZIP)

AUTHOR INFORMATION

Corresponding Authors

Thomas E. Markland − *Department of Chemistry, Stanford University, Stanford, California 94305, United States;* orcid.org/0000-0002-2747-0518; Email: tmarkland@stanford.edu

Steven G. Boxer − *Department of Chemistry, Stanford University, Stanford, California 94305, United States;* orcid.org/0000-0001-9167-4286; Email: sboxer@stanford.edu

Authors

Chu Zheng − *Department of Chemistry, Stanford University, Stanford, California 94305, United States;* orcid.org/0000-0003-3309-208X

Yuezhi Mao − *Department of Chemistry, Stanford University, Stanford, California 94305, United States; Department of Chemistry and Biochemistry, San Diego State University, San Diego, California 92182, United States;* orcid.org/0000-0001-5362-4333

Complete contact information is available at: https://pubs.acs.org/10.1021/jacs.4c18102

Author Contributions

#C.Z. and Y.M. contributed equally to this work. The manuscript was written with contributions from all authors.

Notes

The authors declare no competing financial interest.

ACKNOWLEDGMENTS

We thank Tom Carver at the Stanford Nano Shared Facilities for nickel deposition on Stark windows. This work was supported in part by NIH R35GM118044 (to S.G.B.) and National Science Foundation grant no. CHE-2154291 (to T.E.M.). C.Z. was supported by the Center for Molecular Analysis and Design (CMAD) Fellowship. Y.M. was supported by San Diego State University startup funds. This research also used resources of the National Energy Research Scientific Computing Center (NERSC), a U.S. Department of Energy Office of Science User Facility, using NERSC award BES-ERCAP0028203, and the Sherlock cluster operated by the Stanford Research Computing Center.

ABBREVIATIONS

aEDA, adiabatic energy decomposition analysis; DCM, dichloromethane; DMF, *N*,*N*-dimethylformamide; DMSO, dimethyl sulfoxide; HB, hydrogen bonds; MD, molecular dynamics; QM, quantum mechanical; THF, tetrahydrofuran; VSE, vibrational Stark effect; VSS, vibrational Stark spectroscopy

REFERENCES

(1) Allerhand, A.; Von Rague Schleyer, P. A Survey of CH Groups as Proton Donors in Hydrogen Bonding. *J. Am. Chem. Soc.* **1963**, *85* (12), 1715−1723.

(2) Guerra, C. F.; Bickelhaupt, F. M.; Baerends, E. J. Hydrogen Bonding in Mimics of Watson−Crick Base Pairs Involving C-H Proton Donor and F Proton Acceptor Groups: A Theoretical Study. *ChemPhyschem* **2004**, *5* (4), 481−487.

(3) Desiraju, G. R.; Steiner, T. The Weak Hydrogen Bond. In *Structural Chemistry and Biology*; International Union of Crystal, 2001.

(4) Pullanchery, S.; Kulik, S.; Rehl, B.; Hassanali, A.; Roke, S. Charge Transfer across C-H···O Hydrogen Bonds Stabilizes Oil Droplets in Water. *Science* **2021**, *374* (6573), 1366−1370.

(5) June Sutor, D. The C−H···O Hydrogen Bond in Crystals. *Nature* **1962**, *195* (4836), 68−69.

(6) Jiang, L.; Lai, L. CH···O Hydrogen Bonds at Protein-Protein Interfaces. *J. Biol. Chem.* **2002**, *277* (40), 37732−37740.

(7) Weiss, M. S.; Brandl, M.; Sühnel, J.; Pal, D.; Hilgenfeld, R. More Hydrogen Bonds for the (Structural) Biologist. *Trends Biochem. Sci.* **2001**, *26* (9), 521−523.

(8) Cai, J.; Sessler, J. L. Neutral CH and Cationic CH Donor Groups as Anion Receptors. *Chem. Soc. Rev* **2014**, *43* (17), 6198−6213.
(9) Desiraju, G. R. The C-H···O Hydrogen Bond: Structural Implications and Supramolecular Design. *Acc. Chem. Res.* **1996**, *29* (9), 441−449.
(10) Nishio, M.; Hirota, M.; Umezawa, Y. *The CH/π Interaction: Evidence, Nature, and Consequences*; John Wiley & Sons, 1998.
(11) Hobza, P.; Havlas, Z. Blue-Shifting Hydrogen Bonds. *Chem. Rev.* **2000**, *100* (11), 4253−4264.
(12) Hobza, P.; Havlas, Z. Improper, blue-shifting hydrogen bond. *Theor. Chem. Acc.* **2002**, *108* (6), 325−334.
(13) Mao, Y.; Head-Gordon, M. Probing Blue-Shifting Hydrogen Bonds with Adiabatic Energy Decomposition Analysis. *J. Phys. Chem. Lett.* **2019**, *10* (14), 3899−3905.
(14) Shi, L.; Min, W. Vibrational Solvatochromism Study of the C-H···O Improper Hydrogen Bond. *J. Phys. Chem. B* **2023**, *127* (17), 3798−3805.
(15) Taylor, R.; Kennard, O. Crystallographic Evidence for the Existence of C-H···O, C-H···N, and C-H···Cl Hydrogen Bonds. *J. Am. Chem. Soc.* **1982**, *104*, 5063−5063.
(16) van der Veken, B. J.; Herrebout, W. A.; Szostak, R.; Shchepkin, D. N.; Havlas, Z.; Hobza, P. The Nature of Improper, Blue-Shifting Hydrogen Bonding Verified Experimentally. *J. Am. Chem. Soc.* **2001**, *123* (49), 12290−12293.
(17) Gu, Y.; Kar, T.; Scheiner, S. Fundamental Properties of the CH···O Interaction: Is It a True Hydrogen Bond? *J. Am. Chem. Soc.* **1999**, *121* (40), 9411−9422.
(18) Li, X.; Liu, L.; Schlegel, H. B. On the Physical Origin of Blue-Shifted Hydrogen Bonds. *J. Am. Chem. Soc.* **2002**, *124* (32), 9639−9647.
(19) Pejov, L.; Hermansson, K. On the Nature of Blueshifting Hydrogen Bonds: Ab Initio and Density Functional Studies of Several Fluoroform Complexes. *J. Chem. Phys.* **2003**, *119* (1), 313−324.
(20) Alabugin, I. V.; Manoharan, M.; Peabody, S.; Weinhold, F. Electronic Basis of Improper Hydrogen Bonding: A Subtle Balance of Hyperconjugation and Rehybridization. *J. Am. Chem. Soc.* **2003**, *125* (19), 5973−5987.
(21) Behera, B.; Das, P. K. Blue-Shifted Hydrogen Bonding in the Gas Phase $CH/D_3CN\cdots HCCl_3$ Complexes. *J. Phys. Chem. A* **2019**, *123* (9), 1830−1839.
(22) Delanoye, S. N.; Herrebout, W. A.; van der Veken, B. J. Improper or Classical Hydrogen Bonding? A Comparative Cryosolutions Infrared Study of the Complexes of $HCClF_2$, $HCCl_2F$, and $HCCl_3$ with Dimethyl Ether. *J. Am. Chem. Soc.* **2002**, *124* (25), 7490−7498.
(23) Hobza, P.; Havlas, Z. The Fluoroform···Ethylene Oxide Complex Exhibits a C−H···O Anti-Hydrogen Bond. *Chem. Phys. Lett.* **1999**, *303* (3), 447−452.
(24) Hobza, P.; Špirko, V.; Selzle, H. L.; Schlag, E. W. Anti-Hydrogen Bond in the Benzene Dimer and Other Carbon Proton Donor Complexes. *J. Phys. Chem. A* **1998**, *102* (15), 2501−2504.
(25) Hobza, P.; Špirko, V. R.; Havlas, Z.; Buchhold, K.; Reimann, B.; Barth, H.-D.; Brutschy, B. Anti-Hydrogen Bond between Chloroform and Fluorobenzene. *Chem. Phys. Lett.* **1999**, *299* (2), 180−186.
(26) Joseph, J.; Jemmis, E. D. Red-, Blue-, or No-Shift in Hydrogen Bonds: A Unified Explanation. *J. Am. Chem. Soc.* **2007**, *129* (15), 4620−4632.
(27) Masunov, A.; Dannenberg, J. J.; Contreras, R. H. C−H Bond-Shortening Upon Hydrogen Bond Formation: Influence of an Electric Field. *J. Phys. Chem. A* **2001**, *105* (19), 4737−4740.
(28) Mo, Y.; Wang, C.; Guan, L.; Braïda, B.; Hiberty, P. C.; Wu, W. On the Nature of Blueshifting Hydrogen Bonds. *Chem. − Eur. J.* **2014**, *20* (27), 8444−8452.
(29) Qian, W.; Krimm, S. Vibrational Spectroscopy of Hydrogen Bonding: Origin of the Different Behavior of the C−H···O Hydrogen Bond. *J. Phys. Chem. A* **2002**, *106* (28), 6628−6636.
(30) Zierkiewicz, W.; Jurečka, P.; Hobza, P. On Differences between Hydrogen Bonding and Improper Blue-Shifting Hydrogen Bonding. *ChemPhyschem* **2005**, *6* (4), 609−617.
(31) Fried, S. D.; Boxer, S. G. Measuring Electric Fields and Noncovalent Interactions Using the Vibrational Stark Effect. *Acc. Chem. Res.* **2015**, *48* (4), 998−1006.
(32) Bublitz, G. U.; Boxer, S. G. Stark Spectroscopy: Applications in Chemistry, Biology, and Materials Science. *Annu. Rev. Phys. Chem.* **1997**, *48*, 213−242.
(33) Boxer, S. G. Stark Realities. *J. Phys. Chem. B* **2009**, *113* (10), 2972−2983.
(34) Schneider, S. H.; Boxer, S. G. Vibrational Stark Effects of Carbonyl Probes Applied to Reinterpret IR and Raman Data for Enzyme Inhibitors in Terms of Electric Fields at the Active Site. *J. Phys. Chem. B* **2016**, *120* (36), 9672−9684.
(35) Fried, S. D.; Bagchi, S.; Boxer, S. G. Measuring Electrostatic Fields in Both Hydrogen-Bonding and Non-Hydrogen-Bonding Environments Using Carbonyl Vibrational Probes. *J. Am. Chem. Soc.* **2013**, *135* (30), 11181−11192.
(36) Saggu, M.; Levinson, N. M.; Boxer, S. G. Direct Measurements of Electric Fields in Weak OH···π Hydrogen Bonds. *J. Am. Chem. Soc.* **2011**, *133* (43), 17414−17419.
(37) Saggu, M.; Levinson, N. M.; Boxer, S. G. Experimental Quantification of Electrostatics in X-H···π Hydrogen Bonds. *J. Am. Chem. Soc.* **2012**, *134* (46), 18986−18997.
(38) Zheng, C.; Mao, Y. Z.; Kozuch, J.; Atsango, A.; Ji, Z.; Markland, T. E.; Boxer, S. G. A Two-Directional Vibrational Probe Reveals Different Electric Field Orientations in Solution and an Enzyme Active Site. *Nat. Chem.* **2022**, *14* (8), 891−897.
(39) Luzar, A.; Chandler, D. Hydrogen-Bond Kinetics in Liquid Water. *Nature* **1996**, *379* (6560), 55−57.
(40) Long, Z.; Atsango, A. O.; Napoli, J. A.; Markland, T. E.; Tuckerman, M. E. Elucidating the Proton Transport Pathways in Liquid Imidazole with First-Principles Molecular Dynamics. *J. Phys. Chem. Lett.* **2020**, *11* (15), 6156−6163.
(41) Gutmann, V. Empirical Parameters for Donor and Acceptor Properties of Solvents. *Electrochim. Acta* **1976**, *21* (9), 661−670.
(42) Weinhold, F.; Klein, R. A. What Is a Hydrogen Bond? Mutually Consistent Theoretical and Experimental Criteria for Characterizing H-Bonding Interactions. *Mol. Phys.* **2012**, *110* (9−10), 565−579.
(43) Thompson, W. H.; Hynes, J. T. Frequency Shifts in the Hydrogen-Bonded OH Stretch in Halide−Water Clusters. The Importance of Charge Transfer. *J. Am. Chem. Soc.* **2000**, *122* (26), 6278−6286.
(44) Ramos-Cordoba, E.; Lambrecht, D. S.; Head-Gordon, M. Charge-Transfer and the Hydrogen Bond: Spectroscopic and Structural Implications from Electronic Structure Calculations. *Faraday Discuss* **2011**, *150*, 345−362.
(45) Wang, C.; Danovich, D.; Shaik, S.; Mo, Y. A Unified Theory for the Blue-and Red-Shifting Phenomena in Hydrogen and Halogen Bonds. *J. Chem. Theory Comput.* **2017**, *13* (4), 1626−1637.
(46) Claudino, D.; Mayhall, N. J. Automatic Partition of Orbital Spaces Based on Singular Value Decomposition in the Context of Embedding Theories. *J. Chem. Theory Comput.* **2019**, *15* (2), 1053−1064.
(47) Khaliullin, R. Z.; Head-Gordon, M.; Bell, A. T. An Efficient Self-Consistent Field Method for Large Systems of Weakly Interacting Components. *J. Chem. Phys.* **2006**, *124* (20), 204105.
(48) Mao, Y.; Loipersberger, M.; Horn, P. R.; Das, A.; Demerdash, O.; Levine, D. S.; Prasad Veccham, S.; Head-Gordon, T.; Head-Gordon, M. From Intermolecular Interaction Energies and Observable Shifts to Component Contributions and Back Again: A Tale of Variational Energy Decomposition Analysis. *Annu. Rev. Phys. Chem.* **2021**, *72*, 641−666.
(49) Mao, Y.; Horn, P. R.; Head-Gordon, M. Energy Decomposition Analysis in an Adiabatic Picture. *Phys. Chem. Chem. Phys.* **2017**, *19* (8), 5944−5958.
(50) Shen, H.; Veccham, S. P.; Head-Gordon, M. Exactly Fragment Additive Breakdown of Polarization for Energy Decomposition Analysis Based on the Self-Consistent Field for Molecular Interactions. *J. Chem. Theory Comput.* **2023**, *19* (23), 8624−8638.

https://doi.org/10.1021/jacs.4c18102
J. Am. Chem. Soc. 2025, 147, 6227−6235

(51) Veccham, S. P.; Lee, J.; Mao, Y.; Horn, P. R.; Head-Gordon, M. A Non-Perturbative Pairwise-Additive Analysis of Charge Transfer Contributions to Intermolecular Interaction Energies. *Phys. Chem. Chem. Phys.* **2021**, *23* (2), 928−943.
(52) Lindquist, B. A.; Furse, K. E.; Corcelli, S. A. Nitrile Groups as Vibrational Probes of Biomolecular Structure and Dynamics: An Overview. *Phys. Chem. Chem. Phys.* **2009**, *11* (37), 8119−8132.
(53) Baiz, C. R.; Blasiak, B.; Bredenbeck, J.; Cho, M.; Choi, J. H.; Corcelli, S. A.; Dijkstra, A. G.; Feng, C. J.; Garrett-Roe, S.; Ge, N. H.; et al. Vibrational Spectroscopic Map, Vibrational Spectroscopy, and Intermolecular Interaction. *Chem. Rev.* **2020**, *120* (15), 7152−7218.
(54) Maienschein-Cline, M. G.; Londergan, C. H. The CN Stretching Band of Aliphatic Thiocyanate Is Sensitive to Solvent Dynamics and Specific Solvation. *J. Phys. Chem. A* **2007**, *111* (40), 10020−10025.
(55) Błasiak, B.; Ritchie, A. W.; Webb, L. J.; Cho, M. Vibrational Solvatochromism of Nitrile Infrared Probes: Beyond the Vibrational Stark Dipole Approach. *Phys. Chem. Chem. Phys.* **2016**, *18* (27), 18094−18111.
(56) Kirsh, J. M.; Kozuch, J. Hydrogen Bond Blueshifts in Nitrile Vibrational Spectra Are Dictated by Hydrogen Bond Geometry and Dynamics. *JACS Au* **2024**, *4* (12), 4844−4855.
(57) Wei, L.; Hu, F.; Shen, Y.; Chen, Z.; Yu, Y.; Lin, C. C.; Wang, M. C.; Min, W. Live-Cell Imaging of Alkyne-Tagged Small Biomolecules by Stimulated Raman Scattering. *Nat. Methods* **2014**, *11* (4), 410−412.
(58) Wei, L.; Chen, Z.; Shi, L.; Long, R.; Anzalone, A. V.; Zhang, L.; Hu, F.; Yuste, R.; Cornish, V. W.; Min, W. Super-Multiplex Vibrational Imaging. *Nature* **2017**, *544* (7651), 465−470.
(59) Zhou, L.; Feng, R.-R.; Zhang, W.; Gai, F. Triple-Bond Vibrations: Emerging Applications in Energy and Biological Sciences. *J. Phys. Chem. Lett.* **2024**, *15*, 187−200.
(60) Nyquist, R.; Potts, W. Infrared Absorptions Characteristic of the Terminal Acetylenic Group (-C≡C-H). *Spectrochim. Acta* **1960**, *16* (4), 419−427.
(61) King, G.; So, S. P. Ethynylbenzene; The vibrational spectra of some deuterated isomers. *J. Mol. Spectrosc.* **1970**, *36* (3), 468−487.

https://doi.org/10.1021/jacs.4c18102
J. Am. Chem. Soc. 2025, 147, 6227−6235

Supporting Information

Beyond the Vibrational Stark Effect: Unraveling the Large Redshifts of Alkyne C-H Bond in Solvation Environments

Chu Zheng[1]†, Yuezhi Mao[1,2]†, Thomas E. Markland[1]*, and Steven G. Boxer[1]*

1. Department of Chemistry, Stanford University, Stanford, California 94305, United States.
2. Department of Chemistry and Biochemistry, San Diego State University, San Diego, California 92182, United States
†These authors contributed equally.
*Correspondence to: tmarkland@stanford.edu; sboxer@stanford.edu

Materials and Methods

Chemicals that were used in this work are purchased from the following sources without further purification: hexane (Sigma-Aldrich, 99%), toluene (Sigma-Aldrich, 99.8%), chloroform (Sigma-Aldrich, 99.8%), tetrahydrofuran (Sigma-Aldrich, 99.8%), dichloromethane (Sigma-Aldrich, 99.8%), cyclohexanone (Sigma-Aldrich, 99.8%), dimethyl formamide (Sigma-Aldrich, 99.8%), dimethyl sulfoxide (Sigma-Aldrich, 99.8%), 2-methyl tetrahydrofuran (Sigma-Aldrich, 99%), 1-hexyne (Sigma-Aldrich, 97%), and phenylacetylene (Sigma-Aldrich, 98%).

S1. Vibrational solvatochromism.

As described previously[1-3], 20 mM of the molecule of interest (1-hexyne) was dissolved in a series of solvents. 20 μL of the prepared sample was then injected into a demountable IR cell, which was assembled using two CaF_2 optical windows (19.05 mm diameter, 3 mm thickness, Lambda Research Optics, Inc.) separated by a pair of Teflon spacers (25 μm and 50 μm thick).

FTIR spectra were recorded using a Bruker Vertex 70 spectrometer with a liquid nitrogen-cooled mercury cadmium telluride (MCT) detector (Kolmar Technologies, Inc.) and the sample chamber was constantly purged with dry air to remove atmospheric water. The spectra were recorded in a wavenumber window spanning 4000 – 1000 cm^{-1} with 512 scans at 1 cm^{-1} spectral resolution. The obtained FTIR transmission spectra were converted to the corresponding absorption spectra using the neat solvent spectra taken under similar conditions as the reference. Data collection and processing were performed by the spectroscopy software OPUS 5.0.

S2. Vibrational Stark spectroscopy.

As described previously[1-3], the alkyne molecules of interest were dissolved in 2-methyl THF and added in a Stark cell that was assembled using two CaF_2 optical windows (1 mm thickness, 12.7 mm diameter, FOCtek Photonics) separated by Teflon spacers (~26 μm thick). For each Stark window, a nickel layer of 4.5 nm was deposited on one side (the inner surface on the Stark cell) by which an external electric field can be applied to the Stark cell. Upon adding the sample, the Stark cell was immediately plunged into a customized cryostat[4] filled with liquid nitrogen. The Stark spectra were recorded by a Bruker Vertex 70 spectrometer with 64 scans at 1 cm^{-1} spectral resolution with an external electric field ranging from 0.5 to 1.5 MV/cm, which was applied via a Trek 10/10 high-voltage power amplifier. The obtained Stark spectra were analyzed by a numerical fit using the zeroth, first, and second derivative contributions of the corresponding absorption spectrum or its best-fit Voigt profile as previously described[1-3] to reduce the noise and interference. The Stark tuning rates were determined by the second derivative contribution and reported as $|\Delta\vec{\mu}|f$, where the local field factor f takes into account the difference between the

applied electric field and the actual electric field experienced by the vibrational probe[1-3,5] due to the presence of the frozen-glass matrix.

S3. Fixed-charge MD simulations of alkynes in solvents.

The alkyne molecule of interest was constructed and then geometry-optimized in Gaussian 16[6] using density functional theory (DFT) at the B3LYP/6-311++G(2d,2p) level. The atom coordinates of the optimized structure were then imported into the Antechamber program of AmberTools16[7] for parameterization using the Amber ff99SB-ILDN force field. The obtained force field parameters for the alkyne molecule are shown below. The force field parameters for organic solvents were taken from Caleman et al.[8] All simulations were performed by GROMACS 2018[9] as previously described.[1] Briefly, a single solute molecule was placed in the center of a cubic solvation box (4×4×4 nm^3) filled with solvent molecules. Under periodic boundary conditions, the system was energy-minimized until the maximum force is less than 1000 kJ/mol/nm, followed by NVT and NPT equilibration runs (100 ps for each). MD production runs were performed over 1 ns with 2 fs steps, with a van der Waals cutoff of 10 Å (with analytical vdW correction), an electrostatics cutoff of 10 Å (with particle mesh Ewald method), an SD (leap-frog stochastic dynamics) integrator, the Berendsen thermostat (T = 300 K)[10] and the Parrinello-Rahman barostat (P = 1.0 bar).[11]

S4. Electric field calculations using electronic structure methods

The ensemble-averaged electric field projections on the terminal C—H of 1-hexyne in various solvents were calculated using electronic structure methods based on DFT. For each

solvent, a subset of frames from the MD trajectory was selected for electric field calculations: for solvents that contain no oxygen atoms and form no H-bonds with the alkyne's terminal C—H (hexane, toluene, chloroform, and DCM), 100 evenly-spaced frames were selected from the 1-ns trajectory; for oxygen-containing solvents that can form H-bonds with alkyne's C—H, we first grouped the MD snapshots into HB and non-HB categories based on the cutoff values for $d(C_d \cdots O_a)$ and $\angle H_d\text{-}C_d\text{-}O_a$ determined using the method described in Section S6 and then selected 100 frames from each group for field calculations. Given the selected MD frames, we calculated the solvent electric field on 1-hexyne's terminal C — H using a DFT-based electronic structure partitioning method as documented in our previous work.[12] In brief, we first generated truncated solute-solvent clusters with a cutoff radius 7 Å, i.e., the center-of-mass of each included solvent molecule is within 7 Å of at least one of the atoms in 1-hexyne. We then adopted the subsystem projection atomic orbital decomposition (SPADE)[13] method as a post-processing step of the self-consistent field calculation at the B3LYP/6-31+G(d) level for each truncated solute-solvent complex, which allowed us to assign occupied molecular orbitals (MOs) to the solute and solvent subsystems. The electron density generated from the occupied MOs assigned to the solvent moiety, together with the solvent atomic nuclei, was then employed to evaluate the electric field vectors on the carbon and hydrogen atoms of 1-hexyne's terminal C—H group. For each given snapshot, the solvent electric field projection along the C—H bond ($F_{\mathrm{C-H}}$) is defined as the average of the field projections on the two bonding atoms:

$$F_{\mathrm{C-H}} = \frac{1}{2}(\vec{F}_{\mathrm{C}} \cdot \hat{r}_{\mathrm{C-H}} + \vec{F}_{\mathrm{H}} \cdot \hat{r}_{\mathrm{C-H}})$$

where $\vec{F}_{\mathrm{C}}$ and $\vec{F}_{\mathrm{H}}$ are solvent electric field vectors evaluated at the nuclear positions of atoms C and H, respectively, and $\hat{r}_{\mathrm{C-H}}$ denotes the unit vector along the bond direction. An average over

all selected frames then produces the ensemble-averaged value of $F_{\mathrm{C-H}}$ for each solvent (or for the HB or non-HB population of a given solvent). All the DFT-based electric field calculations were performed using the Q-Chem 5.4 software package.[14]

S5. Adiabatic energy decomposition analysis

We employed the adiabatic energy decomposition analysis (aEDA) based on absolutely localized molecular orbitals (ALMOs)[15-16] to reveal the physical origin of the large frequency shifts of the alkyne's terminal C—H when it is H-bonded to oxygen-containing solvents. This method allows for the decomposition of molecular property shifts arising from noncovalent interactions by introducing two intermediate states between the initial (isolated fragments) and final (geometrically relaxed complex) states of intermolecular binding: (1) the frozen (Frz) state, where monomers interact with each other through permanent electrostatics, Pauli repulsion, and dispersion interaction[17] with no electronic structure relaxation involved; (2) the polarized (Pol) state, which further incorporates the intra-fragment relaxation of each monomer's electronic structure in the presence of other monomers while forbidding charge transfer between them. By relaxing the complex geometry and calculating the molecular properties in these two intermediate states (and the initial and final states), one can decompose the shift in a given molecular property into contributions from frozen interaction (FRZ), polarization (POL), and charge transfer (CT). Using vibrational frequency shifts as an example, we have

$$\Delta\bar{\nu}_{\mathrm{Total}} = \Delta\bar{\nu}_{\mathrm{FRZ}} + \Delta\bar{\nu}_{\mathrm{POL}} + \Delta\bar{\nu}_{\mathrm{CT}}$$

$$\Delta\bar{\nu}_{\mathrm{FRZ}} = \bar{\nu}_{\mathrm{Frz}} - \bar{\nu}_{\mathrm{monomer}}$$

$$\Delta\bar{\nu}_{\mathrm{POL}} = \bar{\nu}_{\mathrm{Pol}} - \bar{\nu}_{\mathrm{Frz}}$$

$$\Delta\bar{\nu}_{\mathrm{CT}} = \bar{\nu}_{\mathrm{Full}} - \bar{\nu}_{\mathrm{Pol}}$$

Here $\Delta\bar{\nu}_{\mathrm{Total}}$ is the total frequency shift upon the formation of an intermolecular complex. By evaluating the frequency of a target vibrational mode (the alkyne's terminal C-H stretch mode in our case) in the isolated monomer state ($\bar{\nu}_{\mathrm{monomer}}$) and those in the frozen ($\bar{\nu}_{\mathrm{Frz}}$) , polarized ($\bar{\nu}_{\mathrm{Pol}}$), and fully relaxed ($\bar{\nu}_{\mathrm{Full}}$) states, one is able to quantify the FRZ, POL, and CT contributions to the overall shift $\Delta\bar{\nu}_{\mathrm{Total}}$. This method has been successfully employed to uncover the physical origins of red- and blue-shifting H-bonds[15-16,18] and frequency shifts of C=O in metal-carbonyl complexes.[19-21]

In this work, we performed ALMO-based aEDA calculations on the H-bonded dimer complexes formed between 1-hexyne and each of the oxygen-containing solvents (THF, cyclohexanone, DMF, and DMSO) to shed light on the vibrational frequency shifts associated with the formation of HBs. All the aEDA-related calculations described below were performed at the ωB97X-V[22]/def2-TZVPD[23-24] level of theory using the release version of Q-Chem 5.4[14]. The harmonic frequencies were scaled by a constant factor of 0.954 based on the recent benchmark by Liang et al.[25] We first identified the minimum-energy configurations of each dimer complex by performing geometry optimizations with varying starting structures. The optimized minimum-energy structures are exhibited in Figure S9, which were all verified to be energy minima by harmonic frequency calculations. The value of $\bar{\nu}_{\mathrm{Full}}$ for each complex was also obtained from this frequency calculation. Then, starting from the fully relaxed structures, we performed geometry optimization followed by harmonic frequency calculations on the polarized and frozen surfaces sequentially, from which the values of $\bar{\nu}_{\mathrm{Pol}}$ and $\bar{\nu}_{\mathrm{Frz}}$ were obtained. Combining $\bar{\nu}_{\mathrm{Full}}$, $\bar{\nu}_{\mathrm{Pol}}$, and

$\bar{\nu}_{\mathrm{Frz}}$ with the harmonic C—H frequency calculated at the relaxed monomer structure of 1-hexyne ($\bar{\nu}_{\mathrm{monomer}}$), we calculated the values of $\Delta\bar{\nu}_{\mathrm{FRZ}}$, $\Delta\bar{\nu}_{\mathrm{POL}}$, and $\Delta\bar{\nu}_{\mathrm{CT}}$ for each HB dimer complex.

To unravel the distance-dependence of the vibrational frequency shift and its decomposition in an HB complex, we further performed ALMO-based aEDA for the 1-hexyne:DMSO complex at varying intermolecular distances. The scanned coordinate, $d(C_d\cdots O_a)$, is illustrated in Figure 5A in the main text. Starting with the equilibrium structure where $d(C_d\cdots O_a)$ = 3.2 Å, we performed a scan of its value from 3.0 Å to 4.6 Å in 0.05 Å intervals. Then, with $d(C_d\cdots O_a)$ constrained at each given value along the scan, we re-optimized the geometry of the complex on the potential energy surfaces associated with the frozen, polarized, and fully relaxed states in the aEDA scheme and performed harmonic frequency analysis to obtain the value of $\bar{\nu}_{\mathrm{CH}}$ in each of these states. These calculations yield the results shown in Figure 5C. We note that since the constraint was only applied to the distance between C_d and O_a, the two monomers were allowed to rotate relative to each other. Such rotations are responsible for the crossing of the "Pol" and "Full" curves between 3.6 and 3.8 Å.

To identify the contribution from the linear VSE to the shift in $\bar{\nu}_{\mathrm{CH}}$, we also calculated the electric field exerted by DMSO on 1-hexyne's terminal C–H bond along the intermolecular distance scan. For these calculations we employed the dimer structures optimized on the fully relaxed surface at each fixed value of $d(C_d\cdots O_a)$. In addition to the SPADE partitioning method that was introduced above, we also evaluated the electric field using the electron density generated from the polarized ALMOs belonging to the DMSO fragment, which serves as an alternative approach to partitioning the electronic structure. These two methods, as in our previous work[12], yielded very similar results at all scanned distances (Figure S8). To be consistent

with the electric field calculations for the solute-solvent complexes (Section S4 above), the electric fields here were also computed at the B3LYP/6-31+G(d) level.

To illustrate the changes in the electronic structure around the C–H bond in the 1-hexyne:DMSO complex during the polarization and charge-transfer processes, we performed the complementary occupied-virtual pairs (COVPs) analysis associated with the recently developed non-perturbative polarization and charge-transfer analysis schemes[26-27]. The COVPs were calculated based on an ALMO-EDA calculation using the optimized minimum-energy structure of the 1-hexyne:DMSO complex at the ωB97X-V/def2-TZVPD level. Note that this is not an adiabatic EDA calculation and does not involve relaxation of the complex geometry. The fragment electrical response function[28] (FERF) approach was employed for the determination of the polarization and charge-transfer energies. The contours of the polarization and charge-transfer COVPs that make the greatest contribution to energy lowering were then visualized with an isovalue 0.04 Å^{-3}. This analysis was performed using a newer version (6.1) of the Q-Chem software package. [14]

S6. Determination of hydrogen bond cutoffs

Since the C—H···O hydrogen bonds are substantially weaker than conventional HBs, the commonly used criterion for H-bonding[29] ($d(C_d \cdots O_a) \leq 3.5$ Å, and $\angle H_d\text{-}C_d\text{-}O_a \leq 30°$) turned out to be unreasonably stringent such that the majority (> 90%) of the MD snapshots would be determined to have no HBs. Here we employed a free-energy-based method[30] to obtain the customized distance and angle cutoffs for the hydrogen bonds formed between 1-hexyne and the oxygen-containing solvents. For each MD snapshot for a given solvent, we first identified the solvent molecule that has the closest contact with 1-hexyne's terminal C–H (as measured by

$d(C_d\cdots O_a)$) and then recorded the $d(C_d\cdots O_a)$ and $\angle H_d\text{-}C_d\text{-}O_a$ values. We then employed the Gaussian kernel density estimation (KDE) method available in SciPy's `stats` module to generate the probability density function $P(r,\theta)$ on a 30×30 2-D grid, where r and θ correspond to $d(C_d\cdots O_a)$ and $\angle H_d\text{-}C_d\text{-}O_a$, respectively. Denoting the maximum probability density as $P_{\max}$ and setting that as the free energy zero point, the free energy (F) at a given pair of r and θ values is given by

$$F(r,\theta) = -k_B T \ln[P(r,\theta)/P_{\max}],$$

where k_B is the Boltzmann constant and T is the temperature (300 K) at which the MD simulations were conducted.

In this work, we set $1k_BT$ as the free energy cutoff for HBs, which corresponds to $P(r,\theta)/P_{\max} = 1/e \approx 0.368$. In Figure S4, we plotted the contour line for $P(r,\theta)/P_{\max} = 0.368$ for all four oxygen-containing solvents. The region inside this contour line corresponds to HB configurations whose free energy is within 0.6 kcal/mol from the most favorable (with minimum free energy) configuration. The greatest r and θ values on this contour line were then adopted as the distance and angle cutoffs r_{cut} and θ_{cut}, respectively. Using the cutoff values obtained, a given MD snapshot will be classified as a H-bonded configuration if $d(C_d\cdots O_a) < r_{\text{cut}}$ and $\angle H_d\text{-}C_d\text{-}O_a < \theta_{\text{cut}}$.

The r_{cut} and θ_{cut} values determined using the procedure described above are shown in Table S8. We then tested two different approaches to determine the average solvent electric field exerted on the alkyne C-H bonds: (i) using the individual cutoff values determined for each solvent; (ii) using the more stringent cutoff values determined for DMSO throughout for all four solvents. Table S5 exhibits the average F_{CH} values calculated using these two approaches: for

cyclohexanone and DMF, approaches (i) and (ii) yield very similar results (20.08 vs. 20.21 MV/cm for cyclohexanone; 25.90 vs. 25.36 MV/cm for DMF), but for THF, the cutoff values obtained for itself are unreasonably loose (with $\theta_{\mathrm{cut}} > 90°$), yielding significantly underestimated average value of F_{CH} for the HB configurations (9.20 vs. 21.23 MV/cm with approaches i and ii). To simplify the discussion, we focused on the average field values calculated using method (ii) in the main text.

Supplementary Figures

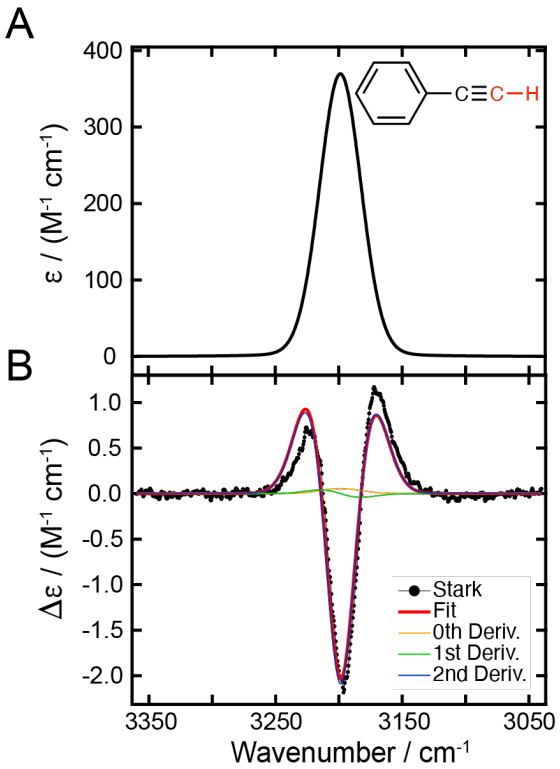

Figure S1. Vibrational Stark spectroscopy of phenylacetylene. (**A**) The infrared absorption spectrum of the terminal C-H vibration of phenylacetylene in 2-methyl THF at 77 K. (**B**) The vibrational Stark spectrum of the terminal C-H vibration scaled to an applied electric field of 1.0 MV/cm with best fits and the 0th, 1st, and 2nd derivative contributions (Table S1).

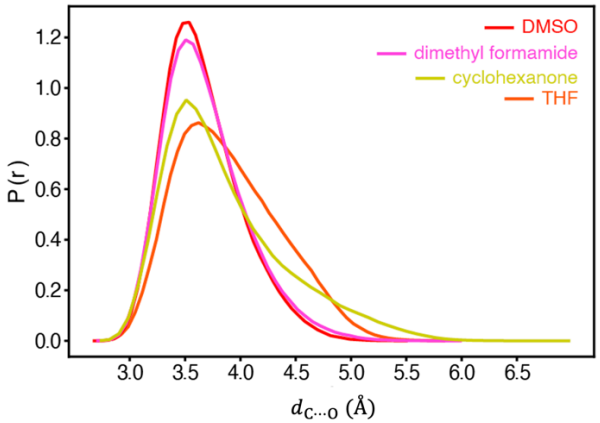

Figure S2. Normalized probability density distribution *P*(d(C_d-O_a)) for 1-hexyne in four oxygen-containing solvents obtained from MD simulations. d (C_d···O_a) (the x-axis) represents the distance between the C atom of 1-hexyne's terminal C–H and the O atom of the nearest-neighbor solvent molecule.

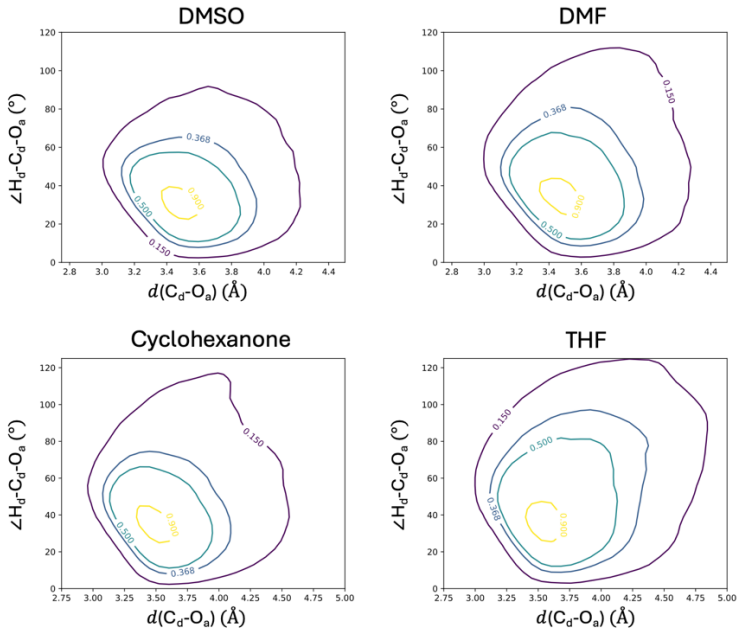

Figure S3. Normalized two-dimensional probability density distribution $P[d(C_d\text{-}O_a), \angle H_d\text{-}C_d\text{-}O_a]$ divided by the maximum probability density P_{max} for 1-hexyne in four oxygen-containing solvents. d (C_d-O_a) (the x-axis) represents the distance between the C atom of 1-hexyne's terminal C–H and the O atom of the nearest-neighbor solvent molecule, and ∠H_d-C_d-O_a (the y-axis) represents the angle between the C-H bond vector and the $C_d\cdots O_a$ axis. The maximum d(C_d-O_a) and ∠H_d-C_d-O_a values on the contour line of value 0.368 ($1/e$) were adopted as the cutoff values to identify HB configurations.

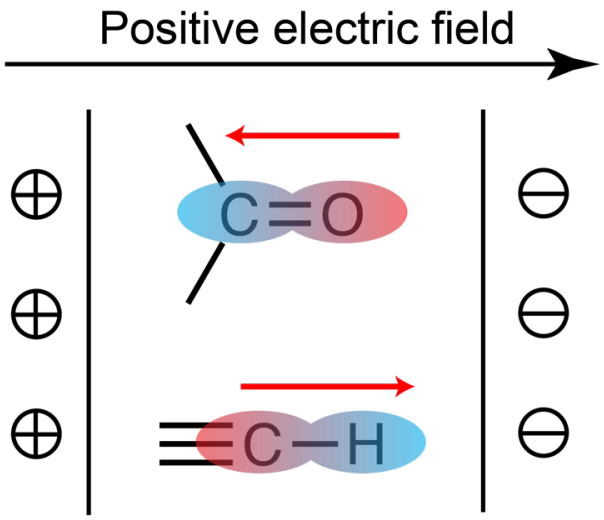

Figure S4. Comparison of the bond dipole direction of C–H and C=O. The red arrows depict the bond dipole directions (pointed from negative partial charge to positive partial charge). A positive electric field along the C=O bond is antiparallel with the C=O bond dipole, resulting in bond destabilization and blueshift. On the other hand, a positive electric field along the alkyne C-H bond stabilizes the bond dipole and thus leads to a redshift in the C-H frequency.

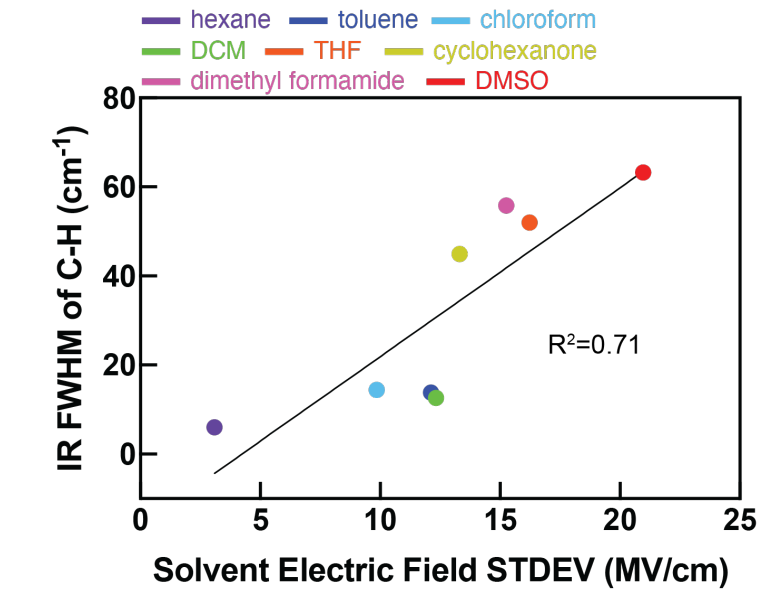

Figure S5. Correlation between the standard deviation of calculated solvent electric fields and the IR linewidth of 1-hexyne's C-H vibration. The least-squares linear fitting gives FWHM(C-H) = 3.8<STDEV> − 16.06 (R^2 = 0.71). The standard deviation of electric fields in oxygen-containing solvents is calculated for the hydrogen-bonded solute population based on the cutoff values of DMSO (Table S5)

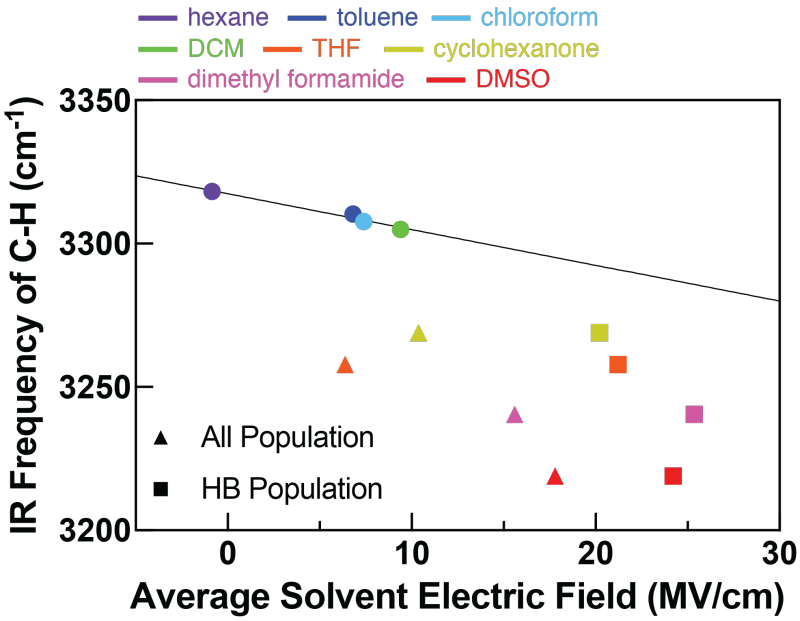

Figure S6. Correlation between the IR frequency of 1-hexyne's C-H vibration ($\bar{\nu}_{CH}$) in solvents and the average solvent electric field. The circles in the plot show the correlation in non-oxygen-containing solvents. The triangles show the correlation between $\bar{\nu}_{CH}$ and the average solvent electric fields exerted on the C-H bond, while the squares show the correlation between $\bar{\nu}_{CH}$ and the average solvent electric fields of the hydrogen-bonded solute population.

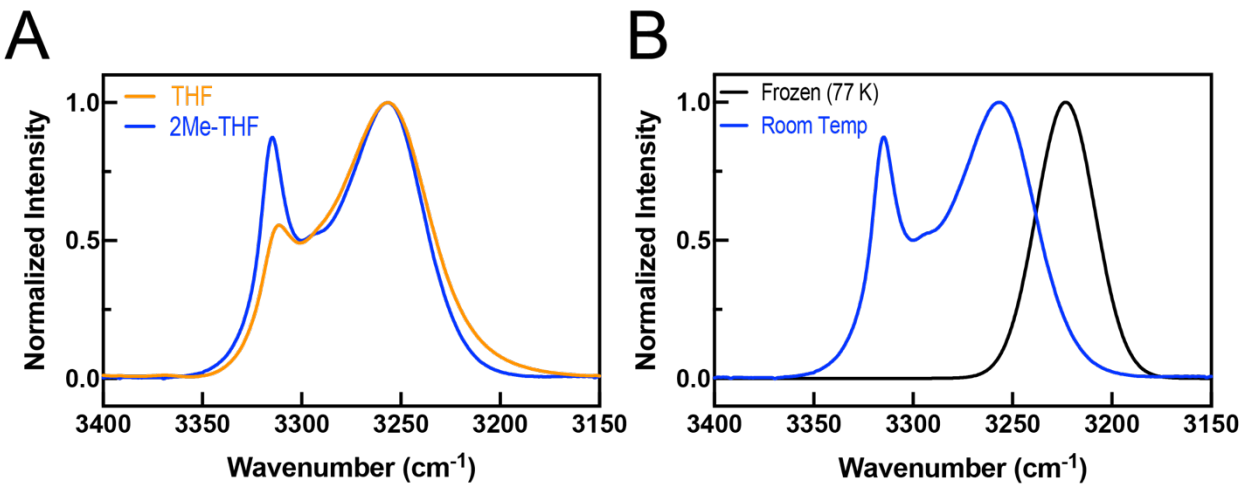

Figure S7. IR spectra of 1-hexyne terminal C-H in THF and 2Me-THF. (**A**) Comparison of the IR spectra of the terminal C-H in liquid THF (orange) and 2Me-THF (blue) at room temperature. (**B**) Comparison of the IR spectra of C-H in liquid 2Me-THF at room temperature (blue) and frozen 2Me-THF at 77 K (black).

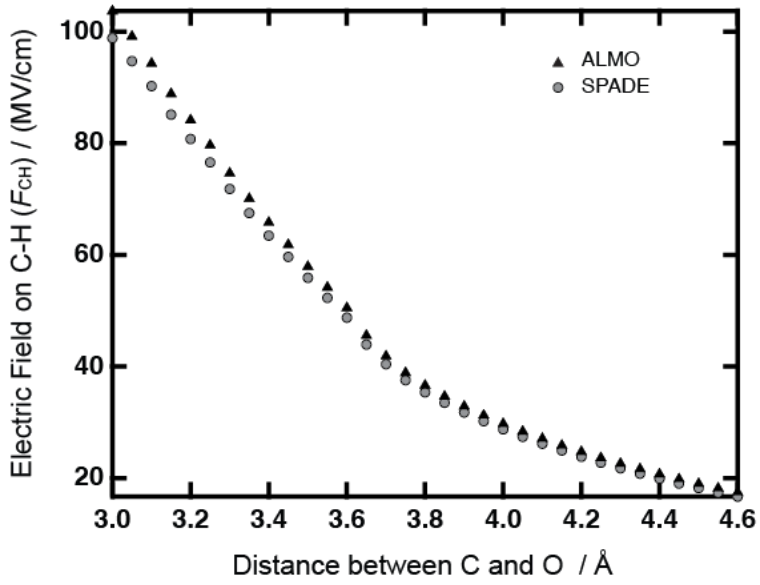

Figure S8. The electric field exerted by the DMSO molecule on 1-hexyne's terminal C–H bond along the scan of the $C_d \cdots O_a$ distance. The field projections were calculated using the dimer structures optimized on the fully relaxed ("Full") surface at the B3LYP/6-31+G(d) level of theory. Two electronic structure partitioning methods, SPADE and ALMO, were used and produced similar results.

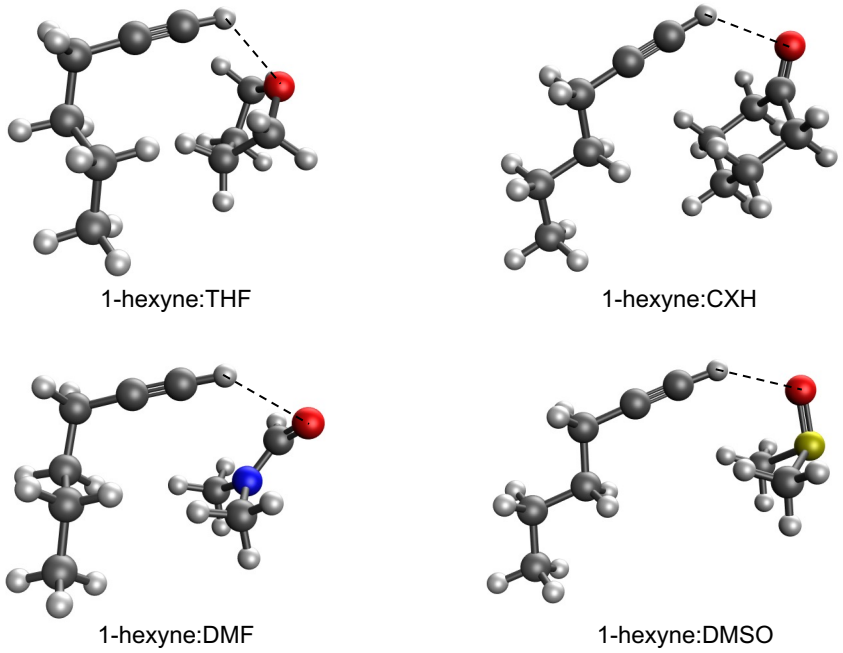

Figure S9. Optimized HB dimer structures of 1-hexyne with THF, cyclohexanone (CXH), dimethyl formamide (DMF), and DMSO in the minimum-energy configurations. The geometry optimizations were performed at the ωB97X-V/def2-TZVPD level.

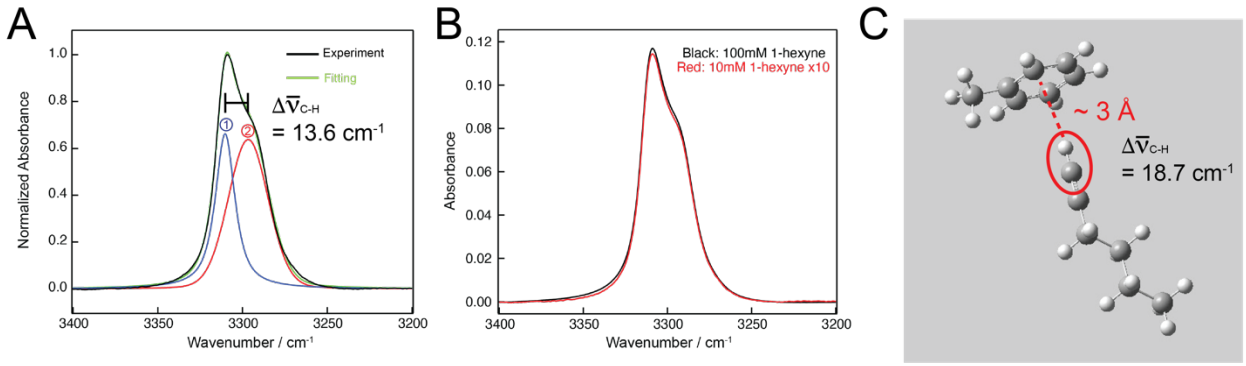

Figure S10. The shoulder IR peak of 1-hexyne's C-H in toluene. (**A**) The IR spectrum of C-H can be fitted by two peaks that are 13.6 cm^{-1} apart. (**B**) The lineshape of 1-hexyne's C-H remains unchanged in the concentration range of 10 and 100mM. The red trace is the 10-times amplified IR spectrum of 10 mM 1-hexyne in toluene, which aligns with the IR spectrum of 100 mM 1-hexyne in toluene. (**C**) Harmonic frequency calculations of a DFT-optimized 1-hexyne:toluene dimer complex at the B3LYP/6-311++G(d,p) level showed a 18.7 cm^{-1} redshift in C–H as a result of the C–H···π interaction. This redshift is in good agreement with the experimentally observed redshift (13.6 cm^{-1}) in Panel A.

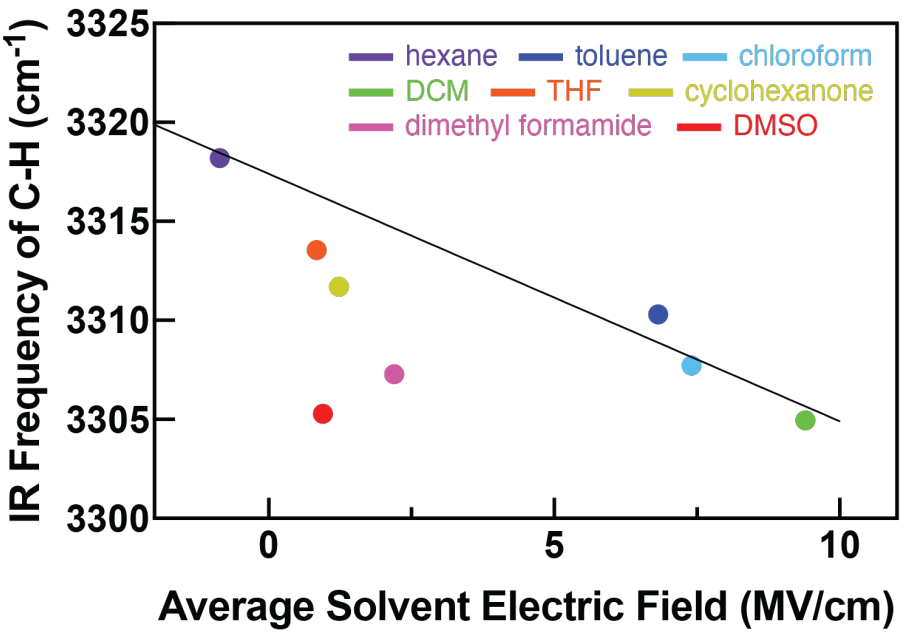

Figure S11. The shoulder IR peaks (Figure 3A) of 1-hexyne's C-H observed in oxygen-containing solvents do not correlate with the ensemble-averaged solvent electric fields calculated based on the non-HB MD configurations (identified using the procedure defined in Section S6). The linear field-frequency correlation was established based on the IR frequencies of C-H and average solvent electric fields in non-oxygen-containing solvents.

Supplementary Tables

Table S1. Vibrational Stark effect data

Vibrational mode	Conc. M	Solvent	Peak position cm^{-1}	FWHM cm^{-1}	A[a]	B cm^{-1}	C cm^{-2}	$\lvert\Delta\vec{\mu}\rvert f$ cm^{-1} / (MV/cm)
1-hexyne C-H	1	2MeTHF	3223.2	34.9	-7.60×10^{-4}	4.55×10^{-3}	0.98	3.13
Phenylacetylene C-H	0.2	2MeTHF	3198.7	38.5	1.48×10^{-4}	2.96×10^{-3}	1.47	3.83

[a] A, B, and C are the fitting coefficients for the Stark spectra, corresponding to the 0th (A), 1st (B), and 2nd (C) derivative contributions respectively.[31] The Stark tuning rates ($|\Delta\mu|f$) can be extracted from the coefficient of the 2nd derivative contribution (C) assuming the difference dipole of the vibrational mode is parallel with its transition dipole moment.[31]

Table S2. FTIR data analysis of 1-hexyne in non-oxygen-containing solvents by curve fit

Solvent	Peak position cm^{-1}	FWHM cm^{-1}
Hexane	3318.1	6.0
Toluene[a]	3310.3	13.8
Chloroform	3307.7	14.4
DCM	3304.7	12.6

[a]The shoulder peak has a peak position at 3296.7 cm^{-1} with FWHM of 27.9 cm^{-1}.

Table S3. FTIR data analysis of 1-hexyne in oxygen-containing solvents by curve fit

Solvent	Shoulder peak		Main peak	
	Peak position cm^{-1}	FWHM cm^{-1}	Peak position cm^{-1}	FWHM cm^{-1}
THF	3291.8	20.5	3257.7	52.0
Cyclohexanone	3309.0	25.9	3268.9	44.9
Dimethyl Formamide	3297.2	33.1	3240.4	55.8
DMSO	3285.7	43.7	3218.9	63.2

Table S4. Nearest-neighbor analysis of MD trajectories for oxygen-containing solvents

Solvent	Most probable $d(C_d \cdots O_a)$ (Å)	Most probable $\angle H_d\text{-}C_d\text{-}O_a$ (°)
THF	3.622	46.13
Cyclohexanone	3.510	41.34
Dimethyl Formamide	3.506	38.58
DMSO	3.537	33.69

Table S5. Average solvent electric fields projected on the C-H of 1-hexyne computed using the SPADE electronic structure partitioning method, with solute-solvent configurations sampled from fixed-charge MD.

Non-hydrogen-bonding solvents						
Solvent	Average F(C-H) (MV/cm)			Standard deviation (MV/cm)		
Hexane	-0.857			3.094		
Toluene	6.822			12.112		
Chloroform	7.404			9.856		
DCM	9.403			12.321		
Hydrogen-bonding solvents						
Solvent	Average F(C-H)[a,c] (MV/cm)	Standard deviation[a,c] (MV/cm)	Average F(C-H)[a,d] (MV/cm)	Standard deviation[a,d] (MV/cm)	Average F(C-H)[b,d] (MV/cm)	Standard deviation[b,d] (MV/cm)
THF	9.20	15.68	21.23	16.23	23.73	15.36
Cyclohexanone	20.08	15.52	20.21	13.31	22.43	13.27
Dimethyl Formamide	25.90	18.64	25.36	15.26	27.51	15.09
DMSO	24.21	20.96	24.21	20.96	27.27	20.92

[a]Electric fields calculated using the SPADE partitioning method.
[b]Electric fields calculated using the ALMO partitioning method.
[c]Electric fields calculated based on HB configurations identified using solvent-specific distance and angle cutoffs.
[d]Electric fields calculated based on HB configurations identified using the cutoff values of DMSO.

Table S6. Adiabatic energy decomposition analysis results for 1-hexyne's terminal C–H stretching frequency[a] in 1-hexyne and electric fields on C-H as changing the distance between 1-hexyne and DMSO.

$d(C_d\cdots O_a)$ (Å)	$\bar{\nu}_{Frz}$ (cm^{-1})	$\bar{\nu}_{Pol}$ (cm^{-1})	$\bar{\nu}_{Full}$ (cm^{-1})	Electric field on C-H (SPADE) (MV/cm)	Electric field on C-H (ALMO) (MV/cm)
3.00	3342.6	3313.4	3226.3	98.835	103.668
3.05	3336.3	3305.8	3226.2	94.715	99.143
3.10	3330.0	3298.6	3227.5	90.243	94.296
3.15	3324.0	3292.2	3231.0	85.119	88.849
3.20	3317.8	3286.4	3234.2	80.765	84.153
3.25	3312.4	3282.0	3237.0	76.567	79.649
3.30	3307.3	3279.1	3242.1	71.812	74.635
3.35	3302.5	3277.6	3247.1	67.490	70.073
3.40	3298.5	3276.1	3251.5	63.457	65.824
3.45	3295.4	3275.2	3255.7	59.646	61.821
3.50	3293.5	3275.2	3260.2	55.898	57.911
3.55	3291.8	3276.6	3265.3	52.310	54.182
3.60	3290.7	3277.8	3270.2	48.770	50.519
3.65	3290.1	3279.6	3280.2	43.965	45.563
3.70	3290.9	3282.5	3285.9	40.422	41.868
3.75	3291.5	3288.8	3290.7	37.576	38.891
3.80	3292.7	3292.0	3292.4	35.407	36.628
3.85	3297.1	3294.3	3294.2	33.522	34.671
3.90	3298.0	3296.5	3295.5	31.801	32.889
3.95	3299.2	3297.6	3296.4	30.229	31.267
4.00	3300.3	3298.1	3297.8	28.769	29.774
4.05	3301.0	3298.9	3298.6	27.426	28.392
4.10	3301.7	3300.0	3299.6	26.173	27.103
4.15	3302.4	3300.6	3300.1	24.978	25.882
4.20	3302.8	3301.4	3300.8	23.856	24.737
4.25	3303.6	3302.0	3301.5	22.793	23.654
4.30	3304.5	3302.6	3302.1	21.787	22.630
4.35	3304.7	3303.2	3302.7	20.832	21.659
4.40	3305.0	3304.1	3303.2	19.927	20.738
4.45	3305.2	3304.2	3303.7	19.062	19.860
4.50	3305.9	3304.8	3304.5	18.246	19.029
4.55	3306.3	3305.2	3305.0	17.433	18.206
4.60	3306.7	3305.7	3305.2	16.723	17.478

[a]The frequency calculation using the same level of theory for the isolated 1-hexyne in vacuo gives $\bar{\nu}_{CH} = 3316.0\ cm^{-1}$. A scaling factor of 0.954[25] has been applied to all the frequency calculation results.

Table S7. Adiabatic EDA results for $\bar{\nu}_{\mathrm{CH}}$[a] in the complexes of 1-hexyne with THF, cyclohexanone (CXH), DMF, and DMSO in the minimum-energy dimer configurations. No geometric constraints were applied in this set of calculations. The rightmost column shows the combined polarization and charge-transfer contribution to the frequency shifts, which are calculated as $\Delta\bar{\nu}_{\mathrm{CH,POL+CT}} = \bar{\upsilon}_{\mathrm{Full}} - \bar{\upsilon}_{\mathrm{Frz}}$ and used as the shift from the "VSE only" to "VSE+POL+CT" points in Figure 5E in the main text.

Solvent	$\bar{\upsilon}_{\mathrm{Frz}}$ (cm^{-1})	$\bar{\upsilon}_{\mathrm{Pol}}$ (cm^{-1})	$\bar{\upsilon}_{\mathrm{Full}}$ (cm^{-1})	$\Delta\bar{\nu}_{\mathrm{CH,POL+CT}}$ (cm^{-1})
THF	3304.2	3297.9	3284.1	-20.1
CXH	3301.4	3295.4	3288.9	-12.5
DMF	3299.0	3290.4	3277.6	-21.4
DMSO	3294.4	3277.9	3234.7	-59.7

[a]The frequency calculation using the same level of theory for the isolated 1-hexyne in vacuo gives $\bar{\nu}_{\mathrm{CH}} = 3316.0\ \mathrm{cm}^{-1}$. A scaling factor of 0.954[25] has been applied to all the frequency calculation results.

Table S8. The distance and angle cutoffs for oxygen-containing solvents determined using the approach described in Section S6.

Solvent	Cutoff for d(C_d···O_a) (Å)	Cutoff for ∠H_d-C_d-O_a (°)
THF	4.38	97.14
Cyclohexanone	4.09	74.55
Dimethyl Formamide	3.98	80.79
DMSO	3.95	65.31

Computational Data

Force Field Parameters for 1-Hexyne

```
[ defaults ]
; nbfunc        comb-rule       gen-pairs       fudgeLJ fudgeQQ
1               2               yes             0.5     0.8333

[ atomtypes ]
;name   bond_type     mass     charge   ptype   sigma         epsilon       Amb
 c3      c3         0.00000  0.00000   A    3.39967e-01   4.57730e-01 ; 1.91  0.1094
 hc      hc         0.00000  0.00000   A    2.64953e-01   6.56888e-02 ; 1.49  0.0157
 c1      c1         0.00000  0.00000   A    3.39967e-01   8.78640e-01 ; 1.91  0.2100
 ha      ha         0.00000  0.00000   A    2.59964e-01   6.27600e-02 ; 1.46  0.0150

[ moleculetype ]
;name            nrexcl
 MOL             3

[ atoms ]
;   nr  type  resi  res  atom  cgnr     charge      mass       ; qtot   bond_type
    1   c3     1    MOL    C    1    -0.093100    12.01000 ; qtot -0.093
    2   hc     1    MOL    H    2     0.033700     1.00800 ; qtot -0.059
    3   hc     1    MOL    H1   3     0.033700     1.00800 ; qtot -0.026
    4   hc     1    MOL    H2   4     0.033700     1.00800 ; qtot 0.008
    5   c3     1    MOL    C1   5    -0.081400    12.01000 ; qtot -0.073
    6   hc     1    MOL    H3   6     0.038700     1.00800 ; qtot -0.035
    7   hc     1    MOL    H4   7     0.038700     1.00800 ; qtot 0.004
    8   c3     1    MOL    C2   8    -0.076400    12.01000 ; qtot -0.072
    9   hc     1    MOL    H5   9     0.047700     1.00800 ; qtot -0.025
   10   hc     1    MOL    H6   10    0.047700     1.00800 ; qtot 0.023
   11   c3     1    MOL    C3   11   -0.004300    12.01000 ; qtot 0.019
   12   hc     1    MOL    H7   12    0.058700     1.00800 ; qtot 0.077
   13   hc     1    MOL    H8   13    0.058700     1.00800 ; qtot 0.136
   14   c1     1    MOL    C4   14   -0.138100    12.01000 ; qtot -0.002
   15   c1     1    MOL    C5   15   -0.162500    12.01000 ; qtot -0.165
   16   ha     1    MOL    H9   16    0.164500     1.00800 ; qtot 0.000

[ bonds ]
;   ai    aj funct   r           k
    1     2   1    1.0969e-01    2.7665e+05 ;     C - H
    1     3   1    1.0969e-01    2.7665e+05 ;     C - H1
    1     4   1    1.0969e-01    2.7665e+05 ;     C - H2
    1     5   1    1.5375e-01    2.5179e+05 ;     C - C1
    5     6   1    1.0969e-01    2.7665e+05 ;    C1 - H3
    5     7   1    1.0969e-01    2.7665e+05 ;    C1 - H4
    5     8   1    1.5375e-01    2.5179e+05 ;    C1 - C2
    8     9   1    1.0969e-01    2.7665e+05 ;    C2 - H5
    8    10   1    1.0969e-01    2.7665e+05 ;    C2 - H6
    8    11   1    1.5375e-01    2.5179e+05 ;    C2 - C3
   11    12   1    1.0969e-01    2.7665e+05 ;    C3 - H7
   11    13   1    1.0969e-01    2.7665e+05 ;    C3 - H8
   11    14   1    1.4671e-01    3.1095e+05 ;    C3 - C4
   14    15   1    1.1983e-01    7.7295e+05 ;    C4 - C5
   15    16   1    1.0668e-01    3.1355e+05 ;    C5 - H9
```

```
[ pairs ]
;  ai    aj   funct
    1     9     1 ;     C - H5
    1    10     1 ;     C - H6
    1    11     1 ;     C - C3
    2     6     1 ;     H - H3
    2     7     1 ;     H - H4
    2     8     1 ;     H - C2
    3     6     1 ;    H1 - H3
    3     7     1 ;    H1 - H4
    3     8     1 ;    H1 - C2
    4     6     1 ;    H2 - H3
    4     7     1 ;    H2 - H4
    4     8     1 ;    H2 - C2
    5    12     1 ;    C1 - H7
    5    13     1 ;    C1 - H8
    5    14     1 ;    C1 - C4
    6     9     1 ;    H3 - H5
    6    10     1 ;    H3 - H6
    6    11     1 ;    H3 - C3
    7     9     1 ;    H4 - H5
    7    10     1 ;    H4 - H6
    7    11     1 ;    H4 - C3
    8    15     1 ;    C2 - C5
    9    12     1 ;    H5 - H7
    9    13     1 ;    H5 - H8
    9    14     1 ;    H5 - C4
   10    12     1 ;    H6 - H7
   10    13     1 ;    H6 - H8
   10    14     1 ;    H6 - C4
   11    16     1 ;    C3 - H9
   12    15     1 ;    H7 - C5
   13    15     1 ;    H8 - C5

[ angles ]
;  ai    aj    ak    funct   theta       cth
    1     5     6     1   1.0980e+02   3.8744e+02 ;     C - C1    - H3
    1     5     7     1   1.0980e+02   3.8744e+02 ;     C - C1    - H4
    1     5     8     1   1.1151e+02   5.2635e+02 ;     C - C1    - C2
    2     1     3     1   1.0758e+02   3.2970e+02 ;     H - C     - H1
    2     1     4     1   1.0758e+02   3.2970e+02 ;     H - C     - H2
    2     1     5     1   1.0980e+02   3.8744e+02 ;     H - C     - C1
    3     1     4     1   1.0758e+02   3.2970e+02 ;    H1 - C     - H2
    3     1     5     1   1.0980e+02   3.8744e+02 ;    H1 - C     - C1
    4     1     5     1   1.0980e+02   3.8744e+02 ;    H2 - C     - C1
    5     8     9     1   1.0980e+02   3.8744e+02 ;    C1 - C2    - H5
    5     8    10     1   1.0980e+02   3.8744e+02 ;    C1 - C2    - H6
    5     8    11     1   1.1151e+02   5.2635e+02 ;    C1 - C2    - C3
    6     5     7     1   1.0758e+02   3.2970e+02 ;    H3 - C1    - H4
    6     5     8     1   1.0980e+02   3.8744e+02 ;    H3 - C1    - C2
    7     5     8     1   1.0980e+02   3.8744e+02 ;    H4 - C1    - C2
    8    11    12     1   1.0980e+02   3.8744e+02 ;    C2 - C3    - H7
    8    11    13     1   1.0980e+02   3.8744e+02 ;    C2 - C3    - H8
    8    11    14     1   1.1171e+02   5.3723e+02 ;    C2 - C3    - C4
    9     8    10     1   1.0758e+02   3.2970e+02 ;    H5 - C2    - H6
    9     8    11     1   1.0980e+02   3.8744e+02 ;    H5 - C2    - C3
   10     8    11     1   1.0980e+02   3.8744e+02 ;    H6 - C2    - C3
```

```
  11    14    15     1   1.7851e+02   4.7028e+02 ;    C3 - C4    - C5
  12    11    13     1   1.0758e+02   3.2970e+02 ;    H7 - C3    - H8
  12    11    14     1   1.0941e+02   4.0501e+02 ;    H7 - C3    - C4
  13    11    14     1   1.0941e+02   4.0501e+02 ;    H8 - C3    - C4
  14    15    16     1   1.7911e+02   3.7070e+02 ;    C4 - C5    - H9

[ dihedrals ] ; propers
; treated as RBs in GROMACS to use combine multiple AMBER torsions per quartet
;   i     j     k     l  func   C0        C1        C2        C3        C4        C5
    1     5     8     9     3   0.66944   2.00832   0.00000  -2.67776   0.00000   0.00000 ;    C-   C1-   C2-   H5
    1     5     8    10     3   0.66944   2.00832   0.00000  -2.67776   0.00000   0.00000 ;    C-   C1-   C2-   H6
    1     5     8    11     3   3.68192   3.09616  -2.09200  -3.01248   0.00000   0.00000 ;    C-   C1-   C2-   C3
    2     1     5     6     3   0.62760   1.88280   0.00000  -2.51040   0.00000   0.00000 ;    H-   C-   C1-   H3
    2     1     5     7     3   0.62760   1.88280   0.00000  -2.51040   0.00000   0.00000 ;    H-   C-   C1-   H4
    2     1     5     8     3   0.66944   2.00832   0.00000  -2.67776   0.00000   0.00000 ;    H-   C-   C1-   C2
    3     1     5     6     3   0.62760   1.88280   0.00000  -2.51040   0.00000   0.00000 ;    H1-   C-   C1-   H3
    3     1     5     7     3   0.62760   1.88280   0.00000  -2.51040   0.00000   0.00000 ;    H1-   C-   C1-   H4
    3     1     5     8     3   0.66944   2.00832   0.00000  -2.67776   0.00000   0.00000 ;    H1-   C-   C1-   C2
    4     1     5     6     3   0.62760   1.88280   0.00000  -2.51040   0.00000   0.00000 ;    H2-   C-   C1-   H3
    4     1     5     7     3   0.62760   1.88280   0.00000  -2.51040   0.00000   0.00000 ;    H2-   C-   C1-   H4
    4     1     5     8     3   0.66944   2.00832   0.00000  -2.67776   0.00000   0.00000 ;    H2-   C-   C1-   C2
    5     8    11    12     3   0.66944   2.00832   0.00000  -2.67776   0.00000   0.00000 ;    C1-   C2-   C3-   H7
    5     8    11    13     3   0.66944   2.00832   0.00000  -2.67776   0.00000   0.00000 ;    C1-   C2-   C3-   H8
    5     8    11    14     3   0.65084   1.95253   0.00000  -2.60338   0.00000   0.00000 ;    C1-   C2-   C3-   C4
    6     5     8     9     3   0.62760   1.88280   0.00000  -2.51040   0.00000   0.00000 ;    H3-   C1-   C2-   H5
    6     5     8    10     3   0.62760   1.88280   0.00000  -2.51040   0.00000   0.00000 ;    H3-   C1-   C2-   H6
    6     5     8    11     3   0.66944   2.00832   0.00000  -2.67776   0.00000   0.00000 ;    H3-   C1-   C2-   C3
    7     5     8     9     3   0.62760   1.88280   0.00000  -2.51040   0.00000   0.00000 ;    H4-   C1-   C2-   H5
    7     5     8    10     3   0.62760   1.88280   0.00000  -2.51040   0.00000   0.00000 ;    H4-   C1-   C2-   H6
    7     5     8    11     3   0.66944   2.00832   0.00000  -2.67776   0.00000   0.00000 ;    H4-   C1-   C2-   C3
    8    11    14    15     3   0.00000   0.00000   0.00000   0.00000   0.00000   0.00000 ;    C2-   C3-   C4-   C5
    9     8    11    12     3   0.62760   1.88280   0.00000  -2.51040   0.00000   0.00000 ;    H5-   C2-   C3-   H7
    9     8    11    13     3   0.62760   1.88280   0.00000  -2.51040   0.00000   0.00000 ;    H5-   C2-   C3-   H8
    9     8    11    14     3   0.65084   1.95253   0.00000  -2.60338   0.00000   0.00000 ;    H5-   C2-   C3-   C4
   10     8    11    12     3   0.62760   1.88280   0.00000  -2.51040   0.00000   0.00000 ;    H6-   C2-   C3-   H7
   10     8    11    13     3   0.62760   1.88280   0.00000  -2.51040   0.00000   0.00000 ;    H6-   C2-   C3-   H8
   10     8    11    14     3   0.65084   1.95253   0.00000  -2.60338   0.00000   0.00000 ;    H6-   C2-   C3-   C4
   11    14    15    16     3   0.00000   0.00000   0.00000   0.00000   0.00000   0.00000 ;    C3-   C4-   C5-   H9
   12    11    14    15     3   0.00000   0.00000   0.00000   0.00000   0.00000   0.00000 ;    H7-   C3-   C4-   C5
   13    11    14    15     3   0.00000   0.00000   0.00000   0.00000   0.00000   0.00000 ;    H8-   C3-   C4-   C5

[ system ]
 MOL

[ molecules ]
; Compound       nmols
 MOL            1
```

Stationary Structures Obtained from Adiabatic EDA Calculations

The calculations were performed at the ωB97X-V/def2-TZVPD level using the Q-Chem 5.4 software package. For each stationary structure obtained, the total energy and the unscaled harmonic frequency for terminal C-H stretch at each stage of the adiabatic EDA procedure (monomer, frozen, polarized, and fully relaxed) are provided.

1-hexyne monomer:

```
16
E_monomer = -234.6103258202 au; omega(CH) = 3475.9 cm-1
C   -0.9809715371   1.5023483852   1.1820370932
C    0.2679375799   2.3932824739   1.2386056501
H   -1.4130452630   1.4002068886   2.1830620983
H   -1.7456042807   1.9763356303   0.5552474912
C    0.8599992107   2.6919542593  -0.1358157822
H   -0.0026491627   3.3339448078   1.7336302545
H    1.0243162546   1.9095092881   1.8681315201
C    2.1028620692   3.5736902807  -0.0535365715
H    1.1056755467   1.7475673571  -0.6344831014
H    0.0985203378   3.1817944151  -0.7566552066
H    1.8752015872   4.5339981412   0.4214760282
H    2.8874624014   3.0891662736   0.5370374508
H    2.5120303880   3.7805519429  -1.0463922648
C   -0.7029907937   0.1619767756   0.6545354646
C   -0.4549746718  -0.9311895805   0.2265746976
H   -0.2420908426  -1.9043752556  -0.1531832398
```

1-hexyne:THF complex:

```
29
E_Frz = -467.0891955291; omega(CH) = 3463.5 cm-1
C    2.5666008285  -1.6245303833  -0.3870791584
C    2.6922415252  -0.1257027972  -0.6960807945
H    2.8003141988  -2.2120453212  -1.2811252777
H    3.2993291784  -1.9085561125   0.3775306326
C    2.5114293587   0.7606383965   0.5332693880
H    3.6790900623   0.0571968922  -1.1385110218
H    1.9503914254   0.1442688128  -1.4579364889
C    2.5718815837   2.2470859296   0.1932227219
H    1.5517002107   0.5263276112   1.0080029110
H    3.2873251003   0.5158257281   1.2701156891
H    2.4455989915   2.8666078991   1.0857042988
H    3.5320833810   2.5097972300  -0.2634929513
H    1.7824949838   2.5176859713  -0.5164276076
C    1.2247480216  -1.9901203531   0.0805850600
C    0.1162339702  -2.2542608523   0.4572731450
H   -0.8745770923  -2.4668023659   0.7934176641
C   -1.9387926253   0.5766496932   1.1440579966
H   -2.5476281397   1.2579067115   1.7535330430
H   -1.1225884145   0.1918744613   1.7634260162
C   -1.4509254290   1.2606209451  -0.1311257382
H   -0.5342488327   0.7816692477  -0.4891696684
```

```
H   -1.2538890588   2.3256893530   0.0135613355
C   -2.6026692965   0.9740783658  -1.0961925091
H   -2.3170051403   1.0405510158  -2.1485737127
H   -3.4328754408   1.6657348016  -0.9181132702
C   -2.9924022665  -0.4416352251  -0.6826850844
H   -2.3702434010  -1.1853459108  -1.2003275773
H   -4.0443574101  -0.6766390562  -0.8687024071
O   -2.7541067377  -0.5213023009   0.7238458076

29
E_Pol = -467.0898574211 au; omega(CH) = 3456.9 cm-1
C    2.5393434708  -1.6221829928  -0.3826186393
C    2.6739179159  -0.1249486798  -0.6959330943
H    2.7722009579  -2.2139522903  -1.2740700816
H    3.2682751273  -1.9078315076   0.3850153594
C    2.4964306255   0.7656700241   0.5308869721
H    3.6619337815   0.0517463550  -1.1382337080
H    1.9338719711   0.1469399828  -1.4590013424
C    2.5563715294   2.2509306810   0.1858147900
H    1.5375246413   0.5332324047   1.0083322509
H    3.2736413113   0.5228351560   1.2669652583
H    2.4338758808   2.8734622660   1.0767420714
H    3.5148664158   2.5117192738  -0.2755712290
H    1.7641599487   2.5194075014  -0.5215518171
C    1.1936163172  -1.9769169265   0.0823517834
C    0.0816096286  -2.2300586337   0.4566363268
H   -0.9146029672  -2.4237323568   0.7898855417
C   -1.9127155897   0.5608919383   1.1460518405
H   -2.5286612735   1.2329122406   1.7585813657
H   -1.0939826139   0.1789697752   1.7638568396
C   -1.4275474221   1.2557282564  -0.1238498950
H   -0.5085471577   0.7822086682  -0.4831869582
H   -1.2351945034   2.3206186883   0.0282601613
C   -2.5776099921   0.9704881979  -1.0911648447
H   -2.2920530774   1.0459986346  -2.1429513343
H   -3.4115042690   1.6564852841  -0.9083156042
C   -2.9599291862  -0.4504907835  -0.6888060451
H   -2.3348174257  -1.1862706383  -1.2142158138
H   -4.0111135531  -0.6890513352  -0.8747745322
O   -2.7182069574  -0.5415407966   0.7168668201

29
E_Full = -467.0909361682 au; omega(CH) = 3442.5 cm-1
C    2.5024680692  -1.6161104610  -0.3727103475
C    2.6530646786  -0.1220761422  -0.6945473360
```

```
H    2.7383869592  -2.2159608152  -1.2579171248
H    3.2209190681  -1.9034132751   0.4041231040
C    2.4716610473   0.7782162609   0.5246114341
H    3.6462160190   0.0439322164  -1.1294184511
H    1.9215528929   0.1506006814  -1.4656714122
C    2.5388401709   2.2605709137   0.1686718832
H    1.5084822073   0.5536315217   0.9975906028
H    3.2431499238   0.5378556204   1.2674675487
H    2.4150217562   2.8902801202   1.0543777519
H    3.5000658650   2.5144872290  -0.2908587116
H    1.7501448947   2.5262144581  -0.5437989492
C    1.1480410199  -1.9517587055   0.0807016146
C    0.0272460158  -2.1813534422   0.4445118348
H   -0.9796814139  -2.3413921603   0.7664826877
C   -1.8768870477   0.5269565636   1.1531635638
H   -2.4888939984   1.1923278621   1.7763825084
H   -1.0575297729   0.1321641841   1.7624073878
C   -1.3905683664   1.2354537014  -0.1085960712
H   -0.4718279373   0.7636134504  -0.4718547599
H   -1.1965762393   2.2982623646   0.0558050432
C   -2.5396505536   0.9629439815  -1.0807456271
H   -2.2519775341   1.0494295057  -2.1311253853
H   -3.3731171865   1.6478760116  -0.8919856533
C   -2.9242500896  -0.4617294940  -0.6950485662
H   -2.2954198195  -1.1919556252  -1.2240088577
H   -3.9743828768  -0.6992365465  -0.8874314881
O   -2.6893442172  -0.5665615926   0.7114242182
```

1-hexyne:cyclohexanone complex:

```
33
E_Frz = -544.5396004498 au; omega(CH) = 3460.6 cm-1
C   -0.1875138412  -2.5758649452   0.0000000000
H   -1.2219466023  -2.8413949713   0.0000000000
C    0.9722550557  -2.2668341201   0.0000000000
C    2.3790964904  -1.8530980483   0.0000000000
C    2.5461298643  -0.3286479439   0.0000000000
C    4.0108361440   0.0984564169   0.0000000000
C    4.1723081840   1.6161683521   0.0000000000
H    2.8765546104  -2.2799192965  -0.8787311183
H    2.8765546104  -2.2799192965   0.8787311183
H    2.0398563609   0.0880671166   0.8791604453
H    2.0398563609   0.0880671166  -0.8791604453
H    4.5129475186  -0.3268556515  -0.8782590722
H    4.5129475186  -0.3268556515   0.8782590722
H    3.7022243067   2.0597947665  -0.8841184604
```

```
H    5.2262786296   1.9075767936   0.0000000000
H    3.7022243067   2.0597947665   0.8841184604
C   -2.6439247054   0.6117027133   1.2786346474
H   -3.3300109757   1.4676106200   1.3470324588
H   -2.8362791072  -0.0484154486   2.1271523631
C   -1.1959310198   1.1247022168   1.2609494936
H   -0.5168760227   0.2650448140   1.3017511299
H   -1.0089271347   1.7230849122   2.1584977662
C   -0.9068716993   1.9399719663   0.0000000000
H    0.1371861240   2.2723760087   0.0000000000
H   -1.5273581749   2.8469555738   0.0000000000
C   -1.1959310198   1.1247022168  -1.2609494936
H   -0.5168760227   0.2650448140  -1.3017511299
H   -1.0089271347   1.7230849122  -2.1584977662
C   -2.6439247054   0.6117027133  -1.2786346474
H   -2.8362791072  -0.0484154486  -2.1271523631
H   -3.3300109757   1.4676106200  -1.3470324588
C   -2.9725771007  -0.1320381502   0.0000000000
O   -3.4490530603  -1.2451603860   0.0000000000


33
E_Pol = -544.5404499958 au; omega(CH) = 3454.3 cm-1
C   -0.2271293122  -2.5440308156   0.0000000000
H   -1.2644087043  -2.8004476177   0.0000000000
C    0.9342227353  -2.2402754817   0.0000000000
C    2.3439943587  -1.8361178008   0.0000000000
C    2.5222932260  -0.3129126988   0.0000000000
C    3.9900328556   0.1034854050   0.0000000000
C    4.1623495936   1.6200044241   0.0000000000
H    2.8384392559  -2.2664733771  -0.8787078497
H    2.8384392559  -2.2664733771   0.8787078497
H    2.0194390333   0.1079553929   0.8792404305
H    2.0194390333   0.1079553929  -0.8792404305
H    4.4889804285  -0.3254975396  -0.8782643439
H    4.4889804285  -0.3254975396   0.8782643439
H    3.6954344598   2.0670060267  -0.8841059710
H    5.2183723846   1.9038600793   0.0000000000
H    3.6954344598   2.0670060267   0.8841059710
C   -2.6201377096   0.5957793833   1.2781983758
H   -3.3103160838   1.4485329910   1.3448115958
H   -2.8099467046  -0.0644748791   2.1272188145
C   -1.1741495746   1.1150393585   1.2608746760
H   -0.4918379193   0.2580574904   1.3008576327
H   -0.9903098303   1.7142739388   2.1585412780
```

```
C   -0.8880359180   1.9313968776   0.0000000000
H    0.1553493390   2.2658876269   0.0000000000
H   -1.5109057167   2.8368432548   0.0000000000
C   -1.1741495746   1.1150393585  -1.2608746760
H   -0.4918379193   0.2580574904  -1.3008576327
H   -0.9903098303   1.7142739388  -2.1585412780
C   -2.6201377096   0.5957793833  -1.2781983758
H   -2.8099467046  -0.0644748791  -2.1272188145
H   -3.3103160838   1.4485329910  -1.3448115958
C   -2.9423876544  -0.1506484015   0.0000000000
O   -3.4069002222  -1.2693423514   0.0000000000

33
E_Full = -544.5414118759; omega(CH) = 3447.5 cm-1
C   -0.2787485643  -2.5040851659   0.0000000000
H   -1.3195695357  -2.7476893310   0.0000000000
C    0.8852857283  -2.2100018206   0.0000000000
C    2.2967124403  -1.8117083752   0.0000000000
C    2.4795168122  -0.2889584019   0.0000000000
C    3.9482455592   0.1234807944   0.0000000000
C    4.1243754407   1.6395674840   0.0000000000
H    2.7896690537  -2.2436737994  -0.8787632048
H    2.7896690537  -2.2436737994   0.8787632048
H    1.9773561836   0.1333855027   0.8791286883
H    1.9773561836   0.1333855027  -0.8791286883
H    4.4460624920  -0.3068144813  -0.8782842490
H    4.4460624920  -0.3068144813   0.8782842490
H    3.6585841208   2.0877480428  -0.8841440530
H    5.1810976207   1.9208122579   0.0000000000
H    3.6585841208   2.0877480428   0.8841440530
C   -2.5824277923   0.5819738623   1.2782638084
H   -3.2619546392   1.4432156456   1.3456884559
H   -2.7801663595  -0.0763496066   2.1270033097
C   -1.1299038656   1.0827855627   1.2605333693
H   -0.4593163878   0.2161004698   1.2981950949
H   -0.9379907938   1.6787675913   2.1587139814
C   -0.8342073280   1.8961706161   0.0000000000
H    0.2133157155   2.2178358786   0.0000000000
H   -1.4460477262   2.8091431171   0.0000000000
C   -1.1299038656   1.0827855627  -1.2605333693
H   -0.4593163878   0.2161004698  -1.2981950949
H   -0.9379907938   1.6787675913  -2.1587139814
C   -2.5824277923   0.5819738623  -1.2782638084
H   -2.7801663595  -0.0763496066  -2.1270033097
H   -3.2619546392   1.4432156456  -1.3456884559
```

```
C   -2.9152821816  -0.1593731348   0.0000000000
O   -3.3964803296  -1.2713714266   0.0000000000
```

1-hexyne:DMF complex:

```
28
E_Frz = -483.1482693825 au; omega(CH) = 3458.0 cm-1
C    2.1229344974  -1.6625645146  -0.7378029497
C    2.5563338926  -0.1896410460  -0.7422236536
H    2.0149473544  -2.0243617252  -1.7658094904
H    2.9016940491  -2.2755179824  -0.2688599858
C    2.8538575263   0.3568765347   0.6513433730
H    3.4477158470  -0.0905109719  -1.3735154883
H    1.7697083310   0.4134221128  -1.2129966332
C    3.2150992805   1.8394184416   0.6292913729
H    1.9828064604   0.1938796832   1.2964025240
H    3.6760084253  -0.2193592524   1.0947255327
H    4.0954470698   2.0226973749   0.0040512083
H    2.3913428404   2.4370679988   0.2234497786
H    3.4344477543   2.2124756166   1.6335299836
C    0.8577720930  -1.8763845899  -0.0256376353
C   -0.1770003763  -2.0206802573   0.5652636633
H   -1.0983011598  -2.1420583152   1.0920010022
C   -1.4446061225   1.4020893761   0.7409598659
H   -1.7946338610   1.0400089592   1.7070104601
H   -0.3774451634   1.1761918779   0.6372815804
H   -1.5849951257   2.4871335680   0.6835701809
N   -2.2043682348   0.7424187254  -0.3014408731
C   -1.8770386806   1.0650231573  -1.6714955255
H   -2.0069665066   2.1367681659  -1.8585851677
H   -0.8385794252   0.7948603997  -1.8981814134
H   -2.5330671674   0.5125438432  -2.3474074285
C   -3.1018178518  -0.2239961843   0.0032007005
H   -3.5854840960  -0.6463130889  -0.8974543528
O   -3.3742534379  -0.6094135733   1.1237966631

28
E_Pol = -483.1491193431 au; omega(CH) = 3449.1 cm-1
C    2.0897571198  -1.7164061999  -0.6718299344
C    2.5341536861  -0.2473157581  -0.7132297770
H    1.9947819049  -2.1078251167  -1.6902191760
H    2.8562800667  -2.3209021801  -0.1727258329
C    2.8247731633   0.3348744464   0.6673010750
H    3.4307405462  -0.1706217373  -1.3402477718
H    1.7546255260   0.3473894190  -1.2063693119
```

```
C    3.1816101192   1.8175038008   0.6097370925
H    1.9521175466   0.1849832418   1.3134392713
H    3.6469202651  -0.2276823226   1.1278628119
H    4.0626719364   1.9880905032  -0.0180790471
H    2.3569163066   2.4025780550   0.1875459827
H    3.3976692568   2.2158497324   1.6049382416
C    0.8114936022  -1.8974213733   0.0260245392
C   -0.2345474464  -2.0130973317   0.6035670033
H   -1.1686354251  -2.1024214041   1.1154045260
C   -1.3787203216   1.3969302369   0.7276204138
H   -1.7298141329   1.0180025497   1.6867778617
H   -0.3157474791   1.1576740849   0.6133058032
H   -1.5045512756   2.4847512958   0.6950542692
N   -2.1522220941   0.7724005190  -0.3267123869
C   -1.8225081666   1.1224091121  -1.6897654230
H   -1.9401336234   2.1996221326  -1.8515153717
H   -0.7872090331   0.8455767245  -1.9224301584
H   -2.4854949880   0.5932656942  -2.3774231295
C   -3.0552054534  -0.1938980083  -0.0436498121
H   -3.5476404956  -0.5876504608  -0.9522953589
O   -3.3249621268  -0.6085831719   1.0680171514

28
E_Full = -483.1500762973 au; omega(CH) = 3435.7 cm-1
C    2.0595296689  -1.7142046909  -0.6676994232
C    2.5053408371  -0.2460632770  -0.7255991825
H    1.9770807110  -2.1211323870  -1.6810752834
H    2.8188735801  -2.3116328531  -0.1494900574
C    2.7843952051   0.3544994828   0.6494917205
H    3.4069172280  -0.1773491959  -1.3462961604
H    1.7296867190   0.3421362515  -1.2328888045
C    3.1256781666   1.8400745375   0.5769606153
H    1.9105109270   0.2028048674   1.2937956769
H    3.6100613244  -0.1945392463   1.1198645735
H    4.0050139806   2.0135922453  -0.0524615937
H    2.2947219803   2.4118272509   0.1487111125
H    3.3372637708   2.2508395295   1.5680683380
C    0.7719192894  -1.8814109628   0.0163519637
C   -0.2821349426  -1.9822510217   0.5824277764
H   -1.2255825764  -2.0521418277   1.0819390613
C   -1.3366430299   1.3596535775   0.7645281861
H   -1.7240297186   0.9961301782   1.7156754775
H   -0.2807245569   1.0802611321   0.6764391258
H   -1.4230417422   2.4509760291   0.7256626617
N   -2.1068177799   0.7613897534  -0.3076220600
```

```
C   -1.7402413881   1.1105634059  -1.6615703275
H   -1.8245855322   2.1915928004  -1.8174304980
H   -0.7082087047   0.8058250181  -1.8741569977
H   -2.4033301450   0.6043764789  -2.3661812404
C   -3.0209075279  -0.2009370981  -0.0500854554
H   -3.5077515156  -0.5754519186  -0.9696593609
O   -3.3058752444  -0.6313515758   1.0524037065
```

1-hexyne:DMSO complex:

```
26
E_Frz = -787.7941330106 au; omega(CH) = 3453.2 cm-1
C   -0.2306224038  -2.1111986307   0.0000000000
H   -1.2838094835  -2.2932720736   0.0000000000
C    0.9477376628  -1.8815112113   0.0000000000
C    2.3800235506  -1.5687689062   0.0000000000
C    2.6539285016  -0.0599351004   0.0000000000
C    4.1458824836   0.2603948284   0.0000000000
C    4.4212461082   1.7614839430   0.0000000000
H    2.8463337376  -2.0294617761  -0.8786832864
H    2.8463337376  -2.0294617761   0.8786832864
H    2.1772428957   0.3906183822   0.8792083951
H    2.1772428957   0.3906183822  -0.8792083951
H    4.6151955137  -0.2011363086  -0.8780982784
H    4.6151955137  -0.2011363086   0.8780982784
H    3.9865028759   2.2396398400  -0.8840168188
H    5.4943827839   1.9716233661   0.0000000000
H    3.9865028759   2.2396398400   0.8840168188
C   -2.1570196586   1.0081810398  -1.3430162519
H   -1.2616614417   0.3901540636  -1.2468365525
H   -2.6766572151   0.7717433135  -2.2729677468
H   -1.9080872132   2.0722475481  -1.3191956873
S   -3.2888301263   0.6258594836   0.0000000000
C   -2.1570196586   1.0081810398   1.3430162519
H   -1.2616614417   0.3901540636   1.2468365525
H   -1.9080872132   2.0722475481   1.3191956873
H   -2.6766572151   0.7717433135   2.2729677468
O   -3.4697775458  -0.8502258707   0.0000000000

26
E_Pol = -787.7953501188 au; omega(CH) = 3436.0 cm-1
C   -0.2972034809  -2.0507971043   0.0000000000
H   -1.3574266809  -2.1963424713   0.0000000000
C    0.8869418772  -1.8512303174   0.0000000000
C    2.3269886656  -1.5757305980   0.0000000000
```

```
C    2.6381214359  -0.0741922609   0.0000000000
C    4.1373245088   0.2107850602   0.0000000000
C    4.4477999282   1.7049558695   0.0000000000
H    2.7816900753  -2.0478145527  -0.8787115323
H    2.7816900753  -2.0478145527   0.8787115323
H    2.1725781570   0.3879222378   0.8793067913
H    2.1725781570   0.3879222378  -0.8793067913
H    4.5955775769  -0.2617106252  -0.8780960589
H    4.5955775769  -0.2617106252   0.8780960589
H    4.0243718397   2.1931308734  -0.8840380055
H    5.5255588949   1.8898737026   0.0000000000
H    4.0243718397   2.1931308734   0.8840380055
C   -2.1152097122   1.0261773665  -1.3430300076
H   -1.2108922122   0.4217027978  -1.2439476371
H   -2.6311515290   0.7808404191  -2.2727600674
H   -1.8818116475   2.0937932361  -1.3209076500
S   -3.2430434181   0.6334312062   0.0000000000
C   -2.1152097122   1.0261773665   1.3430300076
H   -1.2108922122   0.4217027978   1.2439476371
H   -1.8818116475   2.0937932361   1.3209076500
H   -2.6311515290   0.7808404191   2.2727600674
O   -3.4116850775  -0.8453930204   0.0000000000

26
E_Full = -787.7967153755 au; omega(CH) = 3390.7 cm-1
C   -0.3370408395  -1.9333981543   0.0000000000
H   -1.4050984122  -2.0370996910   0.0000000000
C    0.8531660594  -1.7695004021   0.0000000000
C    2.3005902476  -1.5357007709   0.0000000000
C    2.6539830545  -0.0436071834   0.0000000000
C    4.1606192190   0.1995488156   0.0000000000
C    4.5124498768   1.6844872244   0.0000000000
H    2.7417802632  -2.0204462854  -0.8787320071
H    2.7417802632  -2.0204462854   0.8787320071
H    2.2015055857   0.4314326963   0.8792513838
H    2.2015055857   0.4314326963  -0.8792513838
H    4.6055472356  -0.2855622551  -0.8780821550
H    4.6055472356  -0.2855622551   0.8780821550
H    4.1026658249   2.1841905662  -0.8840205100
H    5.5949361069   1.8393994309   0.0000000000
H    4.1026658249   2.1841905662   0.8840205100
C   -2.1282638970   0.9931062405  -1.3434832284
H   -1.2091015603   0.4108873470  -1.2432564155
H   -2.6384314310   0.7349341338  -2.2729351850
H   -1.9217934450   2.0662688087  -1.3214455729
```

```
S   -3.2461647972   0.5749929801   0.0000000000
C   -2.1282638970   0.9931062405   1.3434832284
H   -1.2091015603   0.4108873470   1.2432564155
H   -1.9217934450   2.0662688087   1.3214455729
H   -2.6384314310   0.7349341338   2.2729351850
O   -3.3812891070  -0.9089036426   0.0000000000
```

Stationary Structures Obtained from Gaussian Calculations for the 1-hexyne:toluene Complex

The calculations were performed at the B3LYP/6-311++G(d,p) level using the Gaussian 16 software package. The total energy of the optimized structure and the unscaled harmonic frequency for terminal C-H stretch are provided.

1-hexyne monomer:

```
16
E = -234.666005534 au; omega(CH) = 3477.55 cm-1
C          -4.70202         0.97050         0.02953
H          -4.35078        -0.06448         0.08558
H          -4.33408         1.49457         0.91573
H          -5.79491         0.95209         0.08402
C          -4.22342         1.64841        -1.25740
H          -4.56106         2.69198        -1.26788
H          -3.12711         1.68254        -1.26635
C          -4.71821         0.94364        -2.52426
H          -5.81302         0.91227        -2.52902
H          -4.37857        -0.09763        -2.52742
C          -4.23186         1.63241        -3.81526
H          -3.13585         1.66608        -3.82164
H          -4.56961         2.67562        -3.82321
C          -4.69412         0.97411        -5.03379
C          -5.08473         0.41767        -6.02630
H          -5.42697        -0.06973        -6.90600
```

1-hexyne:toluene complex:

```
31
E(B3LYP/6-311++G(d,p)) = -506.306102691; omega(CH) = 3458.95 cm-1
C          -5.02830         0.72502         0.34849
H          -4.79086        -0.34292         0.31863
H          -4.74317         1.10122         1.33476
H          -6.11424         0.82468         0.25584
C          -4.30577         1.48392        -0.76822
H          -4.53559         2.55369        -0.69061
H          -3.22151         1.39425        -0.62831
```

C	-4.67826	0.98655	-2.16836
H	-5.75884	1.08000	-2.32110
H	-4.44423	-0.07964	-2.25891
C	-3.94690	1.75567	-3.28687
H	-2.86339	1.66541	-3.14345
H	-4.17725	2.82478	-3.20524
C	-4.29069	1.29452	-4.62928
C	-4.58712	0.89990	-5.72673
H	-4.84665	0.55309	-6.69868
C	-6.02264	-1.25251	-9.02991
C	-4.65650	-1.25182	-9.30861
C	-4.02560	-0.07852	-9.71935
C	-4.74231	1.11591	-9.85826
C	-6.11381	1.09943	-9.57929
C	-6.74986	-0.07114	-9.16817
H	-6.51537	-2.16400	-8.71120
H	-4.08096	-2.16539	-9.20740
H	-2.96172	-0.08967	-9.93454
H	-6.68999	2.01331	-9.68447
H	-7.81353	-0.06013	-8.95702
C	-4.04896	2.39285	-10.26846
H	-3.66661	2.92848	-9.39272
H	-3.19948	2.19177	-10.92543
H	-4.73137	3.06641	-10.79200

Additional XYZ coordinates (i) used for solvent electric field calculations and (ii) generated from the intermolecular distance scan for the 1-hexyne:DMSO complex are provided in the supplementary ZIP file.

References

1. Fried, S. D.; Bagchi, S.; Boxer, S. G., Measuring electrostatic fields in both hydrogen-bonding and non-hydrogen-bonding environments using carbonyl vibrational probes. *J. Am. Chem. Soc.* **2013,** *135* (30), 11181-92.

2. Schneider, S. H.; Boxer, S. G., Vibrational Stark Effects of Carbonyl Probes Applied to Reinterpret IR and Raman Data for Enzyme Inhibitors in Terms of Electric Fields at the Active Site. *J Phys Chem B* **2016,** *120* (36), 9672-84.

3. Kozuch, J.; Schneider, S. H.; Zheng, C.; Ji, Z.; Bradshaw, R. T.; Boxer, S. G., Testing the Limitations of MD-Based Local Electric Fields Using the Vibrational Stark Effect in Solution: Penicillin G as a Test Case. *J Phys Chem B* **2021,** *125* (17), 4415-4427.

4. Andrews, S. S.; Boxer, S. G., A liquid nitrogen immersion cryostat for optical measurements. *Rev. Sci. Instrum.* **2000,** *71* (9), 3567-3569.

5. Fried, S. D.; Boxer, S. G., Measuring electric fields and noncovalent interactions using the vibrational stark effect. *Acc. Chem. Res.* **2015,** *48* (4), 998-1006.

6. Frisch, M. J.; Trucks, G. W.; Schlegel, H. B.; Scuseria, G. E.; Robb, M. A.; Cheeseman, J. R., . . . Fox, D. J., Gaussian 16, Revision C.01. Gaussian, Inc.: Wallingford CT, 2016.
7. D.A. Case; R.M. Betz; D.S. Cerutti; T.E. Cheatham, I.; T.A. Darden; R.E. Duke, . . . Kollman, P. A. *AMBER 2016*, University of California, San Francisco, 2016.
8. Caleman, C.; van Maaren, P. J.; Hong, M.; Hub, J. S.; Costa, L. T.; van der Spoel, D., Force Field Benchmark of Organic Liquids: Density, Enthalpy of Vaporization, Heat Capacities, Surface Tension, Isothermal Compressibility, Volumetric Expansion Coefficient, and Dielectric Constant. *J. Chem. Theory Comput.* **2012,** *8* (1), 61-74.
9. Hess, B.; Kutzner, C.; van der Spoel, D.; Lindahl, E., GROMACS 4: Algorithms for Highly Efficient, Load-Balanced, and Scalable Molecular Simulation. *J. Chem. Theory Comput.* **2008,** *4* (3), 435-47.
10. Berendsen, H. J. C.; Postma, J. P. M.; van Gunsteren, W. F.; DiNola, A.; Haak, J. R., Molecular dynamics with coupling to an external bath. *J. Chem. Phys.* **1984,** *81* (8), 3684-3690.
11. Parrinello, M.; Rahman, A., Polymorphic transitions in single crystals: A new molecular dynamics method. *J. Appl. Phys.* **1981,** *52* (12), 7182-7190.
12. Zheng, C.; Mao, Y.; Kozuch, J.; Atsango, A.; Ji, Z.; Markland, T.; Boxer, S., Electric field orientations in solution and enzyme active site revealed by a two-directional vibrational probe. *ChemRxiv. Cambridge: Cambridge Open Engage* **2021**.
13. Claudino, D.; Mayhall, N. J., Automatic Partition of Orbital Spaces Based on Singular Value Decomposition in the Context of Embedding Theories. *J. Chem. Theory Comput.* **2019,** *15* (2), 1053-1064.
14. Epifanovsky, E.; Gilbert, A. T. B.; Feng, X.; Lee, J.; Mao, Y.; Mardirossian, N., . . . Krylov, A. I., Software for the frontiers of quantum chemistry: An overview of developments in the Q-Chem 5 package. *J. Chem. Phys.* **2021,** *155* (8), 084801.
15. Mao, Y.; Loipersberger, M.; Horn, P. R.; Das, A.; Demerdash, O.; Levine, D. S., . . . Head-Gordon, M., From Intermolecular Interaction Energies and Observable Shifts to Component Contributions and Back Again: A Tale of Variational Energy Decomposition Analysis. *Annu. Rev. Phys. Chem.* **2021,** *72*, 641-666.
16. Mao, Y.; Horn, P. R.; Head-Gordon, M., Energy decomposition analysis in an adiabatic picture. *Phys. Chem. Chem. Phys.* **2017,** *19* (8), 5944-5958.
17. Horn, P. R.; Mao, Y.; Head-Gordon, M., Defining the contributions of permanent electrostatics, Pauli repulsion, and dispersion in density functional theory calculations of intermolecular interaction energies. *J Chem Phys* **2016,** *144* (11), 114107.
18. Mao, Y.; Head-Gordon, M., Probing Blue-Shifting Hydrogen Bonds with Adiabatic Energy Decomposition Analysis. *J Phys Chem Lett* **2019,** *10* (14), 3899-3905.
19. Mao, Y.; Ge, Q.; Horn, P. R.; Head-Gordon, M., On the Computational Characterization of Charge-Transfer Effects in Noncovalently Bound Molecular Complexes. *J. Chem. Theory Comput.* **2018,** *14* (5), 2401-2417.
20. Loipersberger, M.; Mao, Y.; Head-Gordon, M., Variational Forward-Backward Charge Transfer Analysis Based on Absolutely Localized Molecular Orbitals: Energetics and Molecular Properties. *J. Chem. Theory Comput.* **2020,** *16* (2), 1073-1089.
21. Rossomme, E.; Lininger, C. N.; Bell, A. T.; Head-Gordon, T.; Head-Gordon, M., Electronic structure calculations permit identification of the driving forces behind frequency shifts in transition metal monocarbonyls. *Phys. Chem. Chem. Phys.* **2020,** *22* (2), 781-798.

22. Mardirossian, N.; Head-Gordon, M., omegaB97X-V: a 10-parameter, range-separated hybrid, generalized gradient approximation density functional with nonlocal correlation, designed by a survival-of-the-fittest strategy. *Phys. Chem. Chem. Phys.* **2014,** *16* (21), 9904-24.
23. Weigend, F.; Ahlrichs, R., Balanced basis sets of split valence, triple zeta valence and quadruple zeta valence quality for H to Rn: Design and assessment of accuracy. *Phys. Chem. Chem. Phys.* **2005,** *7* (18), 3297-305.
24. Rappoport, D.; Furche, F., Property-optimized gaussian basis sets for molecular response calculations. *J Chem Phys* **2010,** *133* (13), 134105.
25. Liang, J.; Feng, X.; Liu, X.; Head-Gordon, M., Analytical harmonic vibrational frequencies with VV10-containing density functionals: Theory, efficient implementation, and benchmark assessments. *J. Chem. Phys.* **2023,** *158* (20).
26. Shen, H.; Veccham, S. P.; Head-Gordon, M., Exactly Fragment Additive Breakdown of Polarization for Energy Decomposition Analysis Based on the Self-Consistent Field for Molecular Interactions. *J. Chem. Theory Comput.* **2023,** *19* (23), 8624-8638.
27. Veccham, S. P.; Lee, J.; Mao, Y.; Horn, P. R.; Head-Gordon, M., A non-perturbative pairwise-additive analysis of charge transfer contributions to intermolecular interaction energies. *Phys. Chem. Chem. Phys.* **2021,** *23* (2), 928-943.
28. Horn, P. R.; Head-Gordon, M., Polarization contributions to intermolecular interactions revisited with fragment electric-field response functions. *J. Chem. Phys.* **2015,** *143* (11).
29. Luzar, A.; Chandler, D., Hydrogen-bond kinetics in liquid water. *Nature* **1996,** *379* (6560), 55-57.
30. Long, Z.; Atsango, A. O.; Napoli, J. A.; Markland, T. E.; Tuckerman, M. E., Elucidating the Proton Transport Pathways in Liquid Imidazole with First-Principles Molecular Dynamics. *J. Phys. Chem. Lett.* **2020,** *11* (15), 6156-6163.
31. Bublitz, G. U.; Boxer, S. G., Stark spectroscopy: applications in chemistry, biology, and materials science. *Annu. Rev. Phys. Chem.* **1997,** *48*, 213-42.